Deep-Sea Research I 70 (2012) 42–59

Contents lists available at SciVerse ScienceDirect

Deep-Sea Research I

journal homepage: www.elsevier.com/locate/dsri

Isotopic model of oceanic silicon cycling: The Kerguelen Plateau case study

Anouk de Brauwere [a,b,*], François Fripiat [c,d], Damien Cardinal [d,e], Anne-Julie Cavagna [b], Fjo De Ridder [f], Luc André [d], Marc Elskens [b]

[a] Université Catholique de Louvain, Institute of Mechanics, Materials and Civil Engineering (IMMC), Louvain-la-Neuve, Belgium
[b] Analytical and Environmental Chemistry & Earth System Sciences, Vrije Universiteit Brussel, Brussels, Belgium
[c] Department of Earth and Environmental Sciences, Université Libre de Bruxelles, Brussels, Belgium
[d] Section of Mineralogy and Petrography, Royal Museum for Central Africa, Tervuren, Belgium
[e] Present address: Laboratoire d'Océanographie et du Climat: Expérimentations et Approches Numériques (LOCEAN), Université Pierre et Marie Curie, Paris, France
[f] VITO-ETE, Mol, Belgium

ARTICLE INFO

Article history:
Received 4 February 2012
Received in revised form
3 August 2012
Accepted 22 August 2012
Available online 1 September 2012

Keywords:
Keops
Kerguelen
Box model
Si isotopes
Uptake
Dissolution
Mixing
Advection

ABSTRACT

A box model is presented describing the time evolution for the three stable Si isotopes (or total concentration and natural isotopic compositions), both in the dissolved and biogenic pools. Temporal variations are controlled by uptake, dissolution (both with isotopic fractionation), settling/export and mixing/advection (without isotopic fractionation). The basic building blocks of the model are combined to form a setup for the Kerguelen Plateau where distinct "plateau" and "out-plateau" areas exist and where measurements were made at the end of the growth season (early 2005, KEOPS cruise: Kerguelen Ocean and Plateau compared Study). In addition, we distinguished between surface (0–100 m) and subsurface (100–400 m) water. This resulted in a model composed of eight compartments, each containing three variables (the three Si isotopes) whose time evolution can be modelled. The model does not assume steady state, and can therefore be used to simulate transient events like blooms. We applied the model to simulate the 2004–2005 growth season. The model parameterisations were kept as simple as possible. Still, the KEOPS measurements were satisfactorily reproduced and estimates of instantaneous and seasonally integrated fluxes compared well with previous literature.

1. Introduction

The modern Si biogeochemical cycle in the ocean is dominated by biogenic silica ($bSiO_2$) production and dissolution. The Si delivered to the ocean passes through the biological uptake and dissolution cycle about 39 times before being removed to the seabed (Treguer et al., 1995; Jin et al., 2006). Diatoms, a phytoplankton group, are the major source of biogenic silica in the ocean, as they form opaline frustules. They are ecologically widespread and have global significance in the carbon and silicon cycles, especially in the Antarctic Circumpolar Current (ACC) south of the Polar Front (PF) where diatoms play a key role in mediating carbon export (Buesseler et al., 2001; Honjo et al., 2008). The ACC diatom productivity, accounting for 20–35% of the global marine biogenic silica production, drives the largest surface oceanic silicic acid ($Si(OH)_4$) latitudinal gradient, from over 60 $\mu mol\,l^{-1}$ south of the PF to less than 5 $\mu mol\,l^{-1}$ north of the PF (Pondaven et al., 2000; Brzezinski et al., 2001; Jin et al., 2006).

In the ocean, especially in the Southern Ocean, biological processes are superimposed onto physical processes, setting the modern oceanic nutrient distribution (Sarmiento et al., 2007). Nutrient-rich deep water masses ascend to the surface mainly south of the PF and a fraction of these waters gains buoyancy to form the so-called Antarctic Surface Water (AASW, Fig. 1). The AASW is transported northward by a net Ekman transport drift under the influence of the westerly winds. Then the AASW mixes with warmer upper-ocean waters to the north mainly via intermediate water mass formation in the northern ACC, supplying nutrients to the low latitude thermocline area (Sarmiento et al., 2004; Watson and Garabato, 2006). Therefore, biological processes occurring in the Southern Ocean have an impact on global biogeochemistry: as a result of the large silicic acid utilization by diatoms in the ACC, the low latitude areas are strongly silicon limited, and this has a significantly impact on the global carbon biological pump (Sarmiento et al., 2004; Matsumoto and Sarmiento, 2008).

Still, large uncertainties are associated with Si-flux estimations owing to (1) the scarcity of the data on biogenic silica production

* Corresponding author at: Université catholique de Louvain, Institute of Mechanics, Materials and Civil Engineering (IMMC), Av. Georges Lemaître 4, BE-1348 Louvain-la-Neuve, Belgium.
E-mail address: anouk.debrauwere@uclouvain.be (A. de Brauwere).

0967-0637/$ - see front matter © 2012 Elsevier Ltd. All rights reserved.
http://dx.doi.org/10.1016/j.dsr.2012.08.004

and dissolution, (2) the difficulty to discriminate between biological and physical processes (Jin et al., 2006), (3) the fact that the interpretation of integrated $bSiO_2$ production-dissolution rates and $bSiO_2$ export is plagued by their strong temporal and spatial variabilities, as well as (4) by artefacts associated with their measurements (e.g., bottle effects, "snapshot" fluxes measurements over 24 h, sediment trap biases, model assumptions). Thus tracers with different sensitivities to physical and biological processes are of great complementary use. Natural silicon isotopic composition is a promising tool to progress on this issue. Si has three stable isotopes and their relative abundances are the result of several distinct processes:

Si-uptake (=$bSiO_2$ production at the seasonal scale): Light ^{28}Si isotopes are preferentially incorporated into biogenic silica with an isotopic fractionation factor ($^{30}\alpha_U$) of 0.9989 ± 0.0004 (De La Rocha et al., 1997) which appears relatively constant across different biogeochemical conditions (e.g., Varela et al., 2004; Alleman et al., 2005; Reynolds et al., 2006; Beucher et al., 2008; Cavagna et al., 2011b). By compiling previous ACC estimates, Fripiat et al. (2011b) refined the mean ACC isotopic fractionation factor to 0.9988 ± 0.0002, which is indistinguishable from the previous estimates but has a reduced standard deviation.

$bSiO_2$ dissolution: During biogenic silica dissolution preferentially light silicon isotopes are released with a fractionation factor ($^{30}\alpha_D$) of 0.99945 (Demarest et al., 2009). This isotopic fractionation counteracts the one occurring during Si-uptake and is about half of its absolute magnitude. By increasing the $bSiO_2$ dissolution-to-production (*D*:*P*) ratio, the overall isotopic fractionation factor for the net biogenic silica production would be dampened (Demarest et al., 2009).

Si supply and removal: Mixing does not fractionate silicon isotopes, the resulting mixing product falls on a mixing line defined by the Si properties of the end-members, i.e., their $Si(OH)_4$ contents and Si isotopic signatures (Fripiat et al., 2011a,b). The biogenic silica produced can sink and be removed from the water column (without isotopic fractionation).

The local Si-isotopic compositions of $bSiO_2$ and $Si(OH)_4$ are a reflection of the combined effect of the above processes, integrated over daily to seasonal timescales.

Since decades biogeochemists use the mass and isotopic balances from short-term (≤ 24 h) stable isotopic tracer incubations (^{13}C, ^{15}N, ^{30}Si) to estimate nutrient uptake and regeneration fluxes, i.e., gross primary production (e.g., Elskens et al., 2002; Cavagna et al., 2011a), *N*-uptake regime (e.g., Dugdale and Goering, 1967; Elskens et al., 2005), and $bSiO_2$ production and dissolution (Nelson and Goering, 1977a,b; de Brauwere et al., 2005; Elskens et al., 2007). By analogy with these short-term incubations, we present a box model for the cycling of the three Si isotopes in silicic acid and biogenic silica between several boxes, over the period of one growing season. While the incubation experiments provide point estimates of the different fluxes, the present model is intended to offer estimates over larger areas and longer periods of time. The structure of the equations is generic and the different terms can be combined according to the application under study. The KEOPS (Kerguelen Ocean and Plateau compared Study) experiment in the Antarctic Zone (AZ) above and east of the Kerguelen Plateau (Blain et al., 2007; Fripiat et al., 2011b) is used as a case study for this model (Fig. 2). The KEOPS model set-up consists of four boxes, representing two horizontal layers and two lateral zones. In each box silicic acid and biogenic silica is modelled, and the compartments are linked by

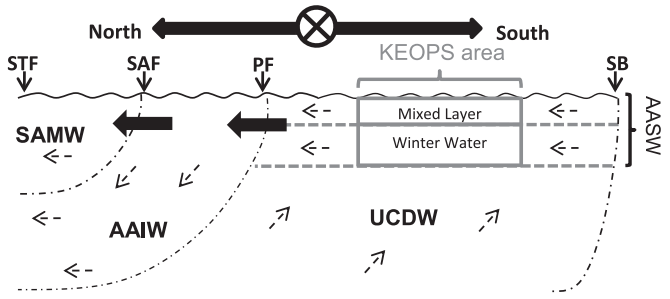

Fig. 1. A schematic view of the meridional overturning circulation in the Antarctic Circumpolar Current, modified from Trull et al. (2001). This is not taking into account complex frontal structures multi-branched as described in Sokolov and Rintoul (2009). UCDW=Upper Circumpolar Deep Water; AAIW=Antarctic Intermediate Water; SAMW=SubAntarctic Mode Water; SB=Southern Boundary; PF=Polar Front; SAF=SubAntarctic Front; STF=SubTropical Front.

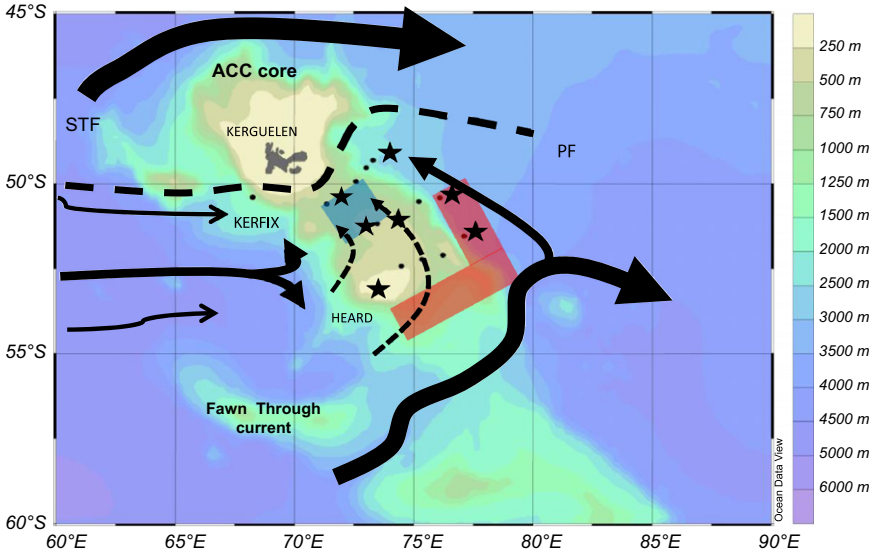

Fig. 2. Map of the study area with bathymetry and geostrophic circulation (black arrows; following Park et al. (2008) and Zhang et al. (2008)). The Fawn Through splits the Kerguelen Plateaus, and constitutes a favoured zonal passage for the circumpolar flow crossing the plateau, "Fawn Through Current" (Park et al., 2008). The KEOPS stations are represented by black dots, while stars refer to the stations with Si-isotopic signatures available in this study. The "plateau" area is defined by the shaded blue area and the "out plateau" area by the shaded red area. (For interpretation of the references to color in this figure legend, the reader is referred to the web version of this article.)

processes of $bSiO_2$ production, dissolution, settling and $Si(OH)_4$ mixing. It is the first attempt to solve the seasonal natural silicon mass and isotopic balances in an oceanic process study by taking into account all these processes simultaneously.

Summarized, the objectives of the study are the following:

(1) Design of a new generic, non-steady state box model for the cycling of Si isotopes and its spatio-temporal variability. The originality of this model lies in the fact that it combines information from natural proxies (delta values), which provide time-integrated signals about ecological processes, with a tracer modelling approach, enabling to quantify exchange rates (fluxes) between the different ecological compartments, both instantaneous and seasonally integrated;
(2) Application of this model to the 2004–2005 growth season in the Kerguelen Plateau area as an illustration of its potential for reproducing the spatio-temporal evolution of Si concentration and composition;
(3) Comparison with the observations made during the KEOPS cruise in order to constrain the values of the model parameters, i.e., allowing a simultaneous estimation of uptake dissolution, settling and mixing fluxes.

The remainder of the manuscript is structured as follows. First, a brief introduction is given on the study domain and the KEOPS campaign (Section 2). In Section 3, the model is described, followed by a whole section discussing how to estimate the values of the rate parameters (Section 4). Putting these pieces of information together allows to present and discuss the modelling results in Section 5. In the final section, the main achievements are summarised.

2. KEOPS study domain and sampling scheme

The methodology followed to measure the natural isotopic composition and the resulting dataset used in this study are described in detail in Fripiat et al. (2011b). Briefly, the KEOPS cruise (19 January to 13 February 2005, aboard R.V. Marion Dufresne; Fig. 2) was conducted to investigate a naturally iron-fertilized area located south-east of the Kerguelen Islands in the Indian sector of the Southern Ocean where a well-developed bloom is observed annually (Blain et al., 2007; Mongin et al., 2008). The cruise track consisted of three transects across the plateau (bathymetry <500 m) and covering a part of the off-plateau high nutrient low Chl-*a* (HNLC) area (bathymetry >1000 m) (Fig. 2). Samples for concentration and silicon isotopic composition of $bSiO_2$ and $Si(OH)_4$ were collected at seven stations.

Following the productivity criteria from Uitz et al. (2009), Fripiat et al. (2011b, this dataset) defined three distinct characteristic areas: the "plateau" area comprising the iron fertilized bloom, the "out-plateau area" located in the HNLC area South-East of the Kerguelen Plateau, and the remaining stations which were in-between these two contrasting groups. In this study, we only distinguish the "plateau" and "out plateau" areas (Fig. 2).

Satellite-derived Chl-*a* data for the 2004–2005 season indicated that the bloom started in early November 2004, reached its maximum in December 2004 and collapsed in February 2005. This means that the KEOPS campaign was conducted during the demise of the bloom just at the onset of the deep winter convective mixing (Mongin et al., 2008).

A typical water mass structure of the AZ upper layer was observed across the KEOPS area (Park et al. (2008), Fig. 1): the mixed layer (ML, depth range=0–100 m), the Winter Water (WW, depth range=100–400 m), and the Upper Circumpolar Deep Water (UCDW, depth range=400–1400 m). The structure of the AZ upper layer displays a seasonal cycle, featuring a single deep convective layer (AASW) in winter, followed in summer by a stratified mixed layer at the surface and a remnant of the deep winter mixed layer below, the so-called Winter Water (WW) (Park et al., 1998).

3. Model description

3.1. Model structure

Fig. 3 shows the general model structure for the KEOPS case study, reflecting the knowledge on the system described above. Four boxes are defined representing two depth zones (surface ML and subsurface WW) and the two KEOPS areas ("plateau" and "out plateau" areas, cf. Section 2). Each spatial box has two compartments: the $Si(OH)_4$ (or dissolved Si, D) and $bSiO_2$ (or biogenic Si, B) pools. In each of these Si pools the three stable isotopes (^{28}Si, ^{29}Si and ^{30}Si) are represented. This results in a total of 24 variables whose time-evolution can be simulated by the model. The isotope concentrations in the different compartments vary with time due to four processes which transfer mass between the pools: uptake, dissolution, settling and $Si(OH)_4$ mixing/advection (cf. the arrows in Fig. 3). Depending on the intensity of each of these processes, the time-evolution of the Si concentrations will be different. One of the main advantages of such a model resides in assessing the result of different process intensities. The model setup providing the closest agreement with field observations may then be interpreted to have the highest probability to be close to "reality". In Section 4, we will discuss in more details the strategy followed to identify the significant processes (amongst the ones considered in the general model, Fig. 3) and to assign a value to the associated model parameters.

3.2. Isotopic notation and fractionation

In biogeochemical studies involving stable isotopes, the relative abundance of the different isotopes are generally expressed using the delta notation. The delta value (in ‰) expresses the ratio of the isotopic ratios of the sample relative to a standard (NBS28 for Si), as follows:

$$\delta^{30}\mathrm{Si} = \left(\frac{\left(^{30}R\right)_{\mathrm{sample}}}{\left(^{30}R\right)_{\mathrm{NBS28}}} - 1 \right) \times 1000 \tag{1}$$

where ^{30}R defines the ^{30}Si:^{28}Si isotopic ratio. Similarly, $\delta\ ^{29}Si$ can be calculated from the $^{29}Si/^{28}Si$ isotopic ratios (^{29}R). The delta value is a relative measurement: only the difference between the isotopic ratios is measured. Therefore it is not necessary to know the real values for the measured isotopic ratios (Cardinal et al., 2003).

Although the field measurements are generally reported in delta-values and total Si concentrations (i.e., the sum of the three isotope concentrations), it was chosen to write the model equations in terms of the isotopic moles (i.e., the concentrations of the isotopes multiplied by the box volumes), because this results in more regular and simple equations. For comparison with the observations the model outputs can always be transformed back into total concentrations and deltas, or vice-versa:

$$\left[^{30}\mathrm{Si}\right] = \frac{\left(^{30}R\right)_{\mathrm{sample}} \times [\mathrm{Si}]}{1 + \left(^{29}R\right)_{\mathrm{sample}} + \left(^{30}R\right)_{\mathrm{sample}}} \tag{2}$$

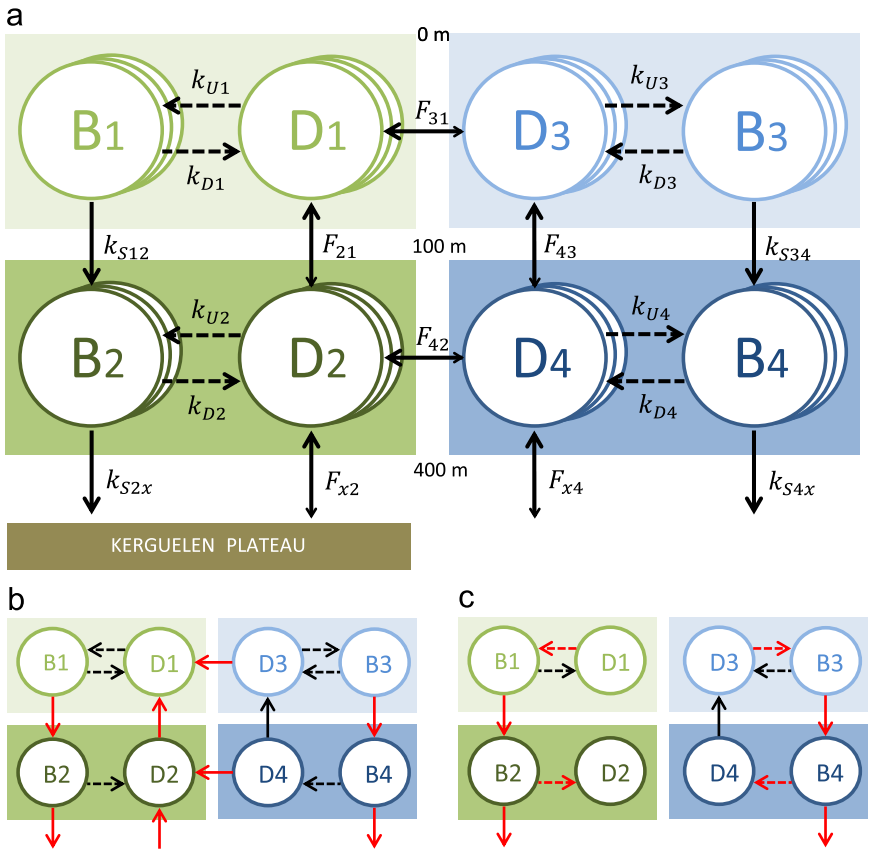

Fig. 3. Schematic representation of the box model for the KEOPS-Si data. Round boxes represent pools of dissolved or biogenic Si. Geographic zones are delimited by rectangles. Arrows stand for processes exchanging Si between the pools, processes subject to isotopic fractionation are indicated by dotted arrows. Mixing/advection fluxes are represented by double arrows because they conceptually represent the net transfer of mass between two pools; the direction indicated by the largest cap corresponds to the direction of positive flux. (a) Total model representing all considered exchange processes; (b) model 1, with the black arrows indicating the processes whose rate parameters are fixed, and red arrows the parameters being optimised; (c) model 2. (For interpretation of the references to color in this figure legend, the reader is referred to the web version of this article.)

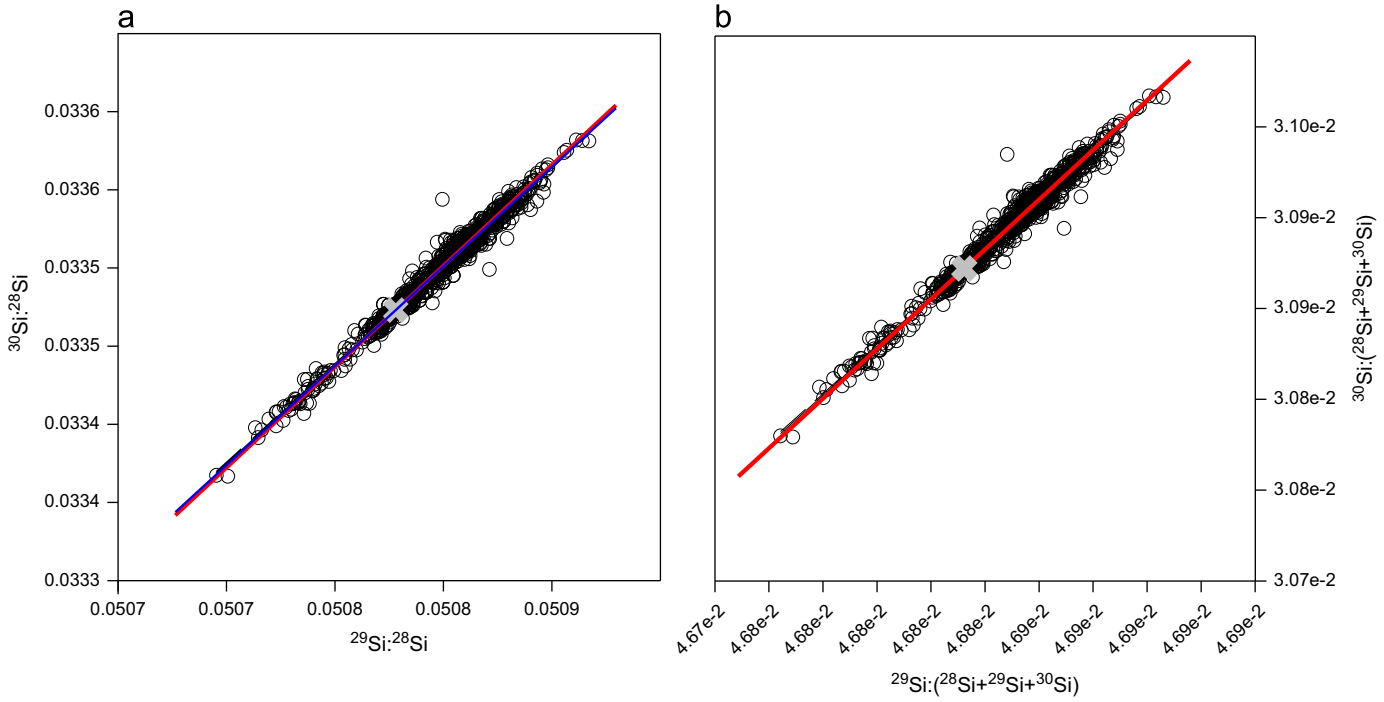

Fig. 4. Relation between the three Si isotopes in terms of (a) isotopic ratios and (b) isotopic abundances. The black dots represents 1000 measurements (rocks, freshwater and marine living diatoms and dissolved silicon) obtained with the MC-ICP-MS (Université Libre de Bruxelles, Belgium) following Abraham et al. (2008) methodology. The gray cross is the crustal isotopic composition (Rosman and Taylor, 1998) and the red and blue lines the isotopic distribution following, respectively, a kinetic or an equilibrium fractionation law (Young et al., 2002). (For interpretation of the references to color in this figure legend, the reader is referred to the web version of this article.)

$$\left[{}^{29}\mathrm{Si}\right] = \frac{\left({}^{29}R\right)_{\mathrm{sample}} \times [Si]}{1+\left({}^{29}R\right)_{\mathrm{sample}}+\left({}^{30}R\right)_{\mathrm{sample}}} \quad (3)$$

$$\left[{}^{28}R\right] = \frac{1 \times [\mathrm{Si}]}{1+\left({}^{30}R\right)_{\mathrm{sample}}+\left({}^{30}R\right)_{\mathrm{sample}}} \quad (4)$$

where $[^{30}\mathrm{Si}]+[^{29}\mathrm{Si}]+[^{28}\mathrm{Si}]=[\mathrm{Si}]$, the total Si concentration. The absolute Si-isotopic ratios from Rosman and Taylor (1998) have been chosen to represent the ${}^{n}R_{\mathrm{NBS28}}$ – 0.033473 and 0.050778 for $^{30}\mathrm{Si}$:$^{28}\mathrm{Si}$ and $^{29}\mathrm{Si}$:$^{28}\mathrm{Si}$, respectively – in order to calculate the ${}^{n}R_{\mathrm{sample}}$ by rearranging Eq. (1).

Si-isotopic fractionation on earth is mass-dependent (Georg et al., 2007; Reynolds et al., 2007) implying a Si-isotopic distribution using a three isotopes plot (30:28 vs. 29:28) on a terrestrial mass fractionation line either using the isotopic ratios (Fig. 4a), the isotopic abundances (Fig. 4b), or delta values (Reynolds et al., 2007). Depending on whether the fractionation is kinetic or at equilibrium, the slope of this line varies (Young et al., 2002). Nevertheless the terrestrial mass fractionation lines estimated either with kinetic or equilibrium isotopic fractionation laws are shown to be undistinguishable in Fig. 4, at least with the current analytical precision on Si isotope measurements.

Kinetic isotopic fractionation implies different reaction rates for the three Si-isotopes when a product is created from a substrate. The light ^{28}Si-bearing molecules are reacting faster than ^{29}Si- or ^{30}Si-bearing molecules and a kinetic isotopic fractionation factor can be computed as follows:

$$\alpha^{30}_{\mathrm{kinetic}} = \frac{k^{30}}{k^{28}} \quad (5)$$

where k^n is the rate constant for the molecules bearing the ^{n}Si isotope. Eq. (5) can be adapted for ^{29}Si and ^{28}Si (for which $\alpha=1$) assuming mass-dependent isotopic fractionation (Young et al., 2002).

Equilibrium isotopic fractionation also implies different reaction rates for the three Si-isotopes but substrate and product are (trans)formed by a forward ($=f$) and backward ($=b$) reaction. The equilibrium fractionation factor can be computed as follows:

$$\alpha^{30}_{\mathrm{equilibrium}} = \frac{\left(k^{30}/k^{28}\right)_f}{\left(k^{30}/k^{28}\right)_b} \quad (6)$$

We decided to use a kinetic isotopic fractionation law for both biogenic silica production and dissolution in the model. For this reason, in the following discussion α^{30} always refers to the kinetic isotopic fractionation factor. For biogenic silica production, this seems to be adequate as $bSiO_2$ is polymerized in a vesicle, called the "silicon vesicle deposit", isolated from the dissolved silicon substrate (Martin-Jezequel et al., 2000). Metabolic balance could modify the extent of the isotopic fractionation depending on where Si-isotopic fractionation occurs and on the ratio of silicic acid entering into and coming out of the cells (Milligan et al., 2004; Fripiat et al., 2012). Since the substrate is removed from the system, the isotopic fractionation cannot be at equilibrium. For $bSiO_2$ dissolution the assumption of kinetic fractionation is more arguable. Although dissolving biogenic silica is directly in contact with the dissolved silicon pool and could theoretically take part in a bidirectional isotopic exchange, equilibrium isotopic fractionation implies that forward and reverse reaction occur at equal rates, which seems unlikely to be the case in the surface ocean as generally there is a measurable $bSiO_2$ dissolution.

3.3. Model equations

The model equations are made up of terms referring to the processes affecting each Si pool. The process term formulations are not specific to the Kerguelen case study, however the way the boxes and processes are combined are. The general model for the KEOPS set-up considers 24 variables (3 isotopes of Si in 8 compartments) and 18 processes, each quantified by one (*a priori* unknown) parameter (Table 1). In addition to these process rate parameters, there are a number of model parameters which are fixed beforehand. This means their value is derived from literature or from external information, and not by matching the model to observations. These fixed model parameters are described and referenced in Table 2. The box areas (in the horizontal) are estimated to be as in Fig. 2 (see Table 2 for the box volumes).

As the measurements available to calibrate the model are rather limited, we wanted to keep the model as simple as possible. But even when staying with simple one-parameter formulations for each process, different choices are still possible. For the uptake process we considered the following three alternatives:

- A zero-order formulation assumes the process to transfer a constant amount of Si per unit of time:

$$\mathrm{uptake}(\mathrm{box}\ i,\mathrm{zero\ order}) = F_{Ui} \quad (7)$$

- A first-order representation implies that the magnitude of the process at each time is proportional to the amount of substrate (D):

$$\mathrm{uptake}(\mathrm{box}\ i,\mathrm{first\ order}) = k_{Ui}D_i \quad (8)$$

- A second-order reaction formulation takes into account the amount of biogenic silica (B), in addition to the dissolved

Table 1
Model variables, processes and rate parameters.

Symbol	**Meaning**				
${}^{n}D_i$	Moles of dissolved ^{n}Si in box i (n=28, 29, 30; i=1, 2, 3, 4).				
${}^{n}B_i$	Moles of biogenic silica ^{n}Si in box i (n=28, 29, 30; i=1, 2, 3, 4).				
Process	**Parameter**	**Meaning**	**Isotopic fractionation**	**Units**	**Reaction order**
Uptake	k_{Ui}	Uptake rate constant for ^{28}Si in box i	Yes	[day^{-1}]	Second
Dissolution	k_{Di}	Dissolution rate constant for ^{28}Si in box i	Yes	[day^{-1}]	First
Sedimentation	k_{Sij}	Sedimentation/export rate constant from box i to j	No	[day^{-1}]	First
Advection/mixing	F_{ij}	Mean mass flux from box i to j	No	[moles day^{-1}]	Zero

Table 2
Fixed model parameters.

Parameter	Meaning	Values	References
α_U^n	Isotopic fractionation factor during uptake for ^{n}Si, to be multiplied with k_{ui} to get uptake rate constant of a specific isotope	$\alpha_U^{28}=1$ $\alpha_U^{29}=0.9994$ $\alpha_U^{30}=0.9989$	De La Rocha et al., 1997
α_D^n	Isotopic fractionation factor during dissolution for ^{n}Si, to be multiplied with k_{Di} to get uptake rate constant of a specific isotope	$\alpha_D^{28}=1$ $\alpha_D^{29}=0.99972$ $\alpha_D^{30}=0.99945$	Demarest et al., 2009
$^nA_{bottom}$	^{n}Si abundance (n=28, 29, 30) assumed for Water coming from below (UCDW abundance)	$^{28}A_{\text{bottom}}=0.92223$ $^{29}A_{\text{bottom}}=0.04686$ $^{30}A_{\text{bottom}}=0.03091$	Fripiat et al., 2011b
V_i	Volume of box i (in liters)	V_1=4.0e15 V_2=1.2e16 V_3=2.0e16 V_4=5.9e16	
T	Time period of simulation (i.e., growth period, in days)	85	Mongin et al., 2008

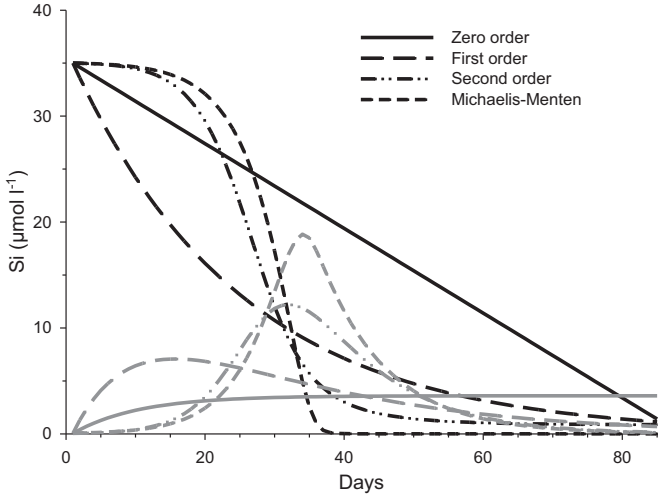

Fig. 5. "Plateau" preliminary simulation assuming Si-uptake by diatoms following zero order (uptake=0.3 µmol Si l^{-1} d^{-1}), first order (k_u=0.0085 d^{-1}), second order ($k_{u'}$=0.004 day^{-1}), and Michaelis–Menten function ($V_{\max}$=0.2 day^{-1}; K_{Si}=10.5 µmol l^{-1}). Biogenic silica dissolution and silicic acid supply have been set to 0. Biogenic silica export has been simulated assuming first order equation in all cases (k_{exp}=0.1 d^{-1}).

substrate as follows:

$$\text{uptake(box } i\text{,second order)} = k'_{Ui} D_i B_i \tag{9}$$

Note that this representation can be interpreted as a pseudo-first order reaction, having a rate constant varying in time ($k'_{Ui}B_i(t)$).

The most suitable reaction order for the uptake process was determined based on a preliminary model test, in which the uptake process is simulated for a simplified KEOPS set-up focusing on the surface layer on the plateau (Fig. 5). Dissolution and mixing/advection ("supply") is neglected, only $bSiO_2$ export is included besides uptake. A Michaelis–Menten saturation function was also tested, in addition to the zero-, first- and second-order formulations (Eqs. (7)–(9)). A Michaelis–Menten saturation function takes into account the maximum uptake capacity ($V_{\max}$) and an affinity ($1/K_{Si}$) for a substrate as follows:

$$\text{uptake(box } i\text{,Michaelis}-\text{Menten)} = \frac{V_{\max}}{K_{Si}+D_i} D_i B_i \tag{10}$$

Although it requires two parameters, we included it in the comparison test because Pondaven et al. (1998) used it to simulate Si-uptake dynamics at the KERFIX station (Fig. 2). Nevertheless, Fig. 5 shows that the second order relationship gives results very similar to the Michaelis–Menten relationship. Therefore, we used a second-order formulation (Eq. (9)) for the uptake processes, because it has the advantage to require only one parameter. Isotopic fractionation is considered in the model by the use of different rate constants for each isotope ($k_U^n = \alpha_U^n k_U$, with n=28, 29, 30 and the reference rate constant $k_U = k_U^{28}$; cf. Eq. (5), Table 2).

$bSiO_2$ dissolution and export were described by first order equations in the model. This formulation is simple but agrees with the intuition that the flux is proportional to the amount of "substrate" (amount present in the pool of origin). This means that when no $bSiO_2$ is present, there is no dissolution or export flux. For dissolution, isotopic fractionation is considered in a similar way as for uptake, but with its own isotopic fractionation factors (see Table 2). For the settling process no isotopic fractionation is assumed, as it is a purely physical phenomenon. However, in reality it is possible that different diatom species with different export efficiencies (Krause et al., 2010) and isotopic compositions result in a pseudo isotopic fractionation of the Si-isotopic signatures, as suggested in Cardinal et al. (2007) and Cavagna et al. (2011b).

Finally, the vertical and lateral "mixing/advection" terms are described by zero-order equations. Theoretically, mass could be transferred between two boxes by mixing/advection in both directions. However, including mixing/advection fluxes in two directions would seriously weigh down the model. In addition, it would be difficult to validate the individual flux values due to very little information generally available on the physical mass transfers. Instead, only one "net" flux is considered (Fig. 3), which will be positive if net mass transfer is in the "default" direction (indicated in Fig. 3 by the largest cap) and negative otherwise. Knowing that the "mixing" fluxes must be interpreted as net mass transfer, it seems inappropriate to parameterise them as first order processes; instead zero-order (constant flux) formulations were chosen. No isotopic fractionation is considered for these fluxes.

Combining the above-discussed choices results in the following equations for box 1 in the KEOPS set-up (for n=28, 29, 30):

$$\frac{dD_1^n}{dt} = -k_{U1}\alpha_U^n D_1^n B_1^n + k_{D1}\alpha_D^n B_1^n + F_{21}\frac{D_2^n}{D_2} + F_{31}\frac{D_3^n}{D_3}, \tag{11}$$

$$\frac{dB_1^n}{dt} = k_{U1}\alpha_U^n D_1^n B_1^n - k_{D1}\alpha_D^n B_1^n - k_{S12} B_1^n, \tag{12}$$

for box 2:

$$\frac{dD_2^n}{dt} = -k_{U2}\alpha_U^n D_2^n B_2^n + k_{D2}\alpha_D^n B_2^n - F_{21}\frac{D_2^n}{D_2} + F_{42}\frac{D_4^n}{D_4} + F_{x2}A_{\text{bottom}}^n, \tag{13}$$

$$\frac{dB_2^n}{dt} = k_{U2}\alpha_U^n D_2^n B_2^n - k_{D2}\alpha_D^n B_2^n + k_{S12}B_1^n - k_{S2x}B_2^n, \quad (14)$$

for box 3:

$$\frac{dD_3^n}{dt} = -k_{U3}\alpha_U^n D_3^n B_3^n + k_{D3}\alpha_D^n B_3^n + F_{43}\frac{D_4^n}{D_4} - F_{31}\frac{D_3^n}{D_3}, \quad (15)$$

$$\frac{dB_3^n}{dt} = k_{U3}\alpha_U^n D_3^n B_3^n - k_{D3}\alpha_D^n B_3^n - k_{S34}B_3^n, \quad (16)$$

and for box 4:

$$\frac{dD_4^n}{dt} = -k_{U4}\alpha_U^n D_4^n B_4^n + k_{D4}\alpha_D^n B_4^n - F_{42}\frac{D_4^n}{D_4} - F_{43}\frac{D_4^n}{D_4} + F_{x4}A_{\text{bottom}}^n, \quad (17)$$

$$\frac{dB_4^n}{dt} = k_{U4}\alpha_U^n D_4^n B_4^n - k_{D4}\alpha_D^n B_4^n + k_{S34}B_3^n - k_{S4x}B_4^n \quad (18)$$

The symbols are explained in Fig. 3, Tables 1 and 2). The equations were integrated using the MATLAB (4,5) Runge–Kutta solver, in order to simulate the time evolution of the 24 state variables. By matching these modelled Si concentrations to the measured values (at the end of the bloom), we can now (try to) estimate the values of the 18 unknown rate parameters (the *k*'s and *F*'s), i.e., investigate the importance of the different processes. The followed procedure to do this is described in Section 4.

Note that by including equations for all three isotopes we do not pretend that they behave independently (cf. Section 3.2). Nevertheless, it is valuable to include the three in the model, because the measurements are available and every additional measurement brings some additional information. In the worst case, the measurements of the two isotopic compositions are like "replicates" of the same quantity. The number of unknown rate parameters does not increase by adding or removing the equations of one isotope (cf. Eqs. (11)–(18)).

3.4. Integrated flux for each process

For given parameter values, the total (seasonally integrated) molar flux of each process can be found by integrating over the simulation period (*T*). For the export flux (in moles), this boils down to:

export flux from box *i* to *j*

$$= k_{Sij}\left(\int_0^T B_i^{28}(t)dt + \int_0^T B_i^{29}(t)dt + \int_0^T B_i^{30}(t)dt\right). \quad (19)$$

For the uptake and dissolution processes, we also have to take the isotopic fractionation into account:

uptake flux in box *i*

$$= k_{Ui}\left(\int_0^T \alpha_U^{28} D_i^{28}(t)dt + \int_0^T \alpha_U^{29} D_i^{29}(t)dt + \int_0^T \alpha_U^{30} D_i^{30}(t)dt\right) \quad (20)$$

dissolution flux in box *i*

$$= k_{Di}\left(\int_0^T \alpha_D^{28} B_i^{28}(t)dt + \int_0^T \alpha_D^{29} B_i^{29}(t)dt + \int_0^T \alpha_D^{30} B_i^{30}(t)dt\right). \quad (21)$$

As mixing/advection are described using zero-order equations, multiplying the mixing/advection parameter by the time period gives the integrated fluxes in moles.

3.5. Determination of box-averaged values

The major assumption underlying any box model is that each box is homogeneous, and consequently can be characterized by a single concentration (i.e., in this case for every given time for each isotope). However, in every box, water is sampled at several stations and several depths (Fig. 2). Therefore, the question arises which single value must be assigned for each box. According to the box model assumption, the chosen values must be representative for the "central tendency" of the boxes. In addition to this central value, an estimate of the range of internal variability is required to know up to which precision the model must fit the measurements. If all the measurements within one box are symmetrically distributed, both the mean and the median are appropriate metrics to represent the "central tendency". Otherwise, the median should preferably be used (Daszykowski et al., 2007). For every compartment, mean, median, standard deviation, interquartile range and skewness of the measurements were computed (Table 3).

The mean and the median are generally very close; therefore both are probably appropriate metrics for characterizing the boxes' concentrations and isotopic compositions. Nevertheless, the skewness metric indicates that the data are not always distributed in a symmetric way. The standard deviations and 3/4 × the interquartile range (i.e., the difference between the 75th and the 25th percentile) should be similar if the measurements are (approximately) normally distributed. In most cases, the standard deviation is higher. Therefore, we used the interquartile range as a measure of the dispersion and the median value as central box value. Note that the interquartile range thus only represents the variability of the measurements within a compartment, and does not account explicitly for the analytical precision. Remarkably, the within-box interquartile range × 3/4 (=1 standard deviation in the case of a normal distribution) found for the delta values is of the same order of magnitude as the analytical precision, generally reported to be 0.1‰ (1 SD). However, the analytical uncertainty could be considerably higher than this value, at least according to inter-laboratory comparisons (Reynolds et al., 2007). In other words, the uncertainty range that we use in this study to assess the model fit is a lower bound estimate of the real uncertainty that could be associated with the median box values.

3.6. Initial conditions and bloom period

Eqs. (11)–(18) must be integrated (in time) in order to find the time evolution of [^{28}Si], [^{29}Si] and [^{30}Si] in each compartment. According to our objectives, we would like to integrate over the whole period of the 2004–2005 growth season. In other words, the number of moles of each isotope in each compartment at the onset of (or just before) the bloom must be given (i.e., the initial conditions), as well as the bloom period. The rationale for defining these values is given in this section.

The temporal evolution of the silicon isotopes in the "out plateau" area reflects the seasonal dynamics described for the AZ in Section 2 (Fripiat et al., 2011b): (1) the WW is representative of the mixed layer Si-source, and (2) the WW is an interface where the final summer ML and UCDW mix together during the winter convective mixing, to generate a homogenous layer in the upper 400 m, constituting the AASW. Consequently, the "out plateau" WW is assumed to be representative of the initial conditions (just before the bloom), both in the surface and subsurface "out plateau" boxes (boxes 3 and 4).

For the "plateau" area there are two possible initial conditions:

(1) Owing to the rapid (~3 months) ventilation of the water masses above the plateau coming mainly from the "out plateau" area (Park et al., 2008), the "out plateau" WW could be representative of the initial conditions in the "plateau" area as well (Fripiat et al., 2011b). A summer alteration of the WW above the plateau was suggested by Fripiat et al. (2011b) and it was hypothesized to result mainly from a subsurface Si-uptake during the growth period.
(2) At the KERFIX station (see Fig. 2 for the location) – and during a different year than the KEOPS cruise – Pondaven et al., 1998

Table 3
Statistical properties of the measurements within each box. Stations A3-1, A3-2, B1 are used for boxes 1 and 2, while stations B11, C11-1, C11-2 are used for boxes 3 and 4 (see Fripiat et al., 2011b).

Box	Species	Data	Mean	Median	Skewness	Standard deviation	Interquartile range*3/4
1	$Si(OH)_4$ (μM)	10	2.11	1.79	1.10	1.03	0.81
	$\delta^{29}Si_{Si(OH)_4}$ (‰)	3	1.31	1.30	1.73	0.02	0.01
	$\delta^{30}Si_{Si(OH)_4}$ (‰)	3	2.56	2.51	1.73	0.09	0.06
	$bSiO_2$ (μM)	11	3.08	3.12	0.14	1.12	1.22
	δ^{29} Si_{bSiO_2} (‰)	7	1.13	1.11	−0.20	0.11	0.10
	$\delta^{30}Si_{bSiO_2}$ (‰)	7	2.29	2.26	−0.03	0.15	0.17
2	$Si(OH)_4$ (μM)	16	34.5	33.9[a]	−0.15	16.9	20.6
	$\delta^{29}Si_{Si(OH)_4}$ (‰)	13	0.95	0.96[a]	−0.56	0.13	0.15
	δ $^{30}Si_{Si(OH)_4}$ (‰)	13	1.85	1.87[a]	−0.61	0.25	0.18
	$bSiO_2$ (μM)	35	4.70	2.90[a]	2.26	4.40	3.00
	$\delta^{29}Si_{bSiO_2}$ (‰)	3	0.94	0.94[a]	−1.49	0.02	0.01
	δ $^{30}Si_{bSiO_2}$ (‰)	3	1.90	1.96[a]	−1.73	0.10	0.06
3	$Si(OH)_4$ (μM)	11	27.2	25.9	1.11	2.26	2.04
	$\delta^{29}Si_{Si(OH)_4}$ (‰)	12	1.12	1.14	−0.31	0.08	0.09
	$\delta^{30}Si_{Si(OH)_4}$ (‰)	12	2.19	2.22	−0.72	0.14	0.12
	$bSiO_2$ (μM)	12	2.02	1.88	0.82	0.56	0.51
	$\delta^{29}Si_{bSiO_2}$ (‰)	10	0.57	0.56	0.03	0.06	0.03
	$\delta^{30}Si_{bSiO_2}$ (‰)	10	1.14	1.13	0.44	0.15	0.10
4	$Si(OH)_4$ (μM)	14	57.4	57.4[b]	−0.25	14.1	17.2
	$\delta^{29}Si_{Si(OH)_4}$ (‰)	12	0.78	0.79[b]	0.38	0.06	0.06
	$\delta^{30}Si_{Si(OH)_4}$ (‰)	13	1.50	1.51[b]	0.22	0.11	0.12
	$bSiO_2$ (μM)	23	1.31	0.97[b]	1.12	0.90	0.75
	$\delta^{29}Si_{bSiO_2}$ (‰)	4	0.55	0.55[b]	−0.47	0.08	0.05
	$\delta^{30}Si_{bSiO_2}$ (‰)	4	1.08	1.09[b]	−0.60	0.08	0.05

[a] Values used as initial conditions for box 1 and 2 (WW plateau).
[b] Values used as initial conditions for box 3 and 4 (WW out-plateau).

measured a subsurface WW $Si(OH)_4$ concentration close to the "plateau" WW. This implies that there is a significantly different WW west of the plateau which could be a more relevant Si-source for the "plateau" WW (see Table 3 for characteristics).

After testing the different possibilities, it appeared that the best results were found with initial conditions (2), and hence these conditions are used for the results shown below. This is also in agreement with the measurement from the recent KEOPS2 cruise at the same place in November 2011, showing silicic acid concentration in the "plateau" WW not significantly different from conditions (2) (Blain, 2012, personal communication). Starting from these initial conditions, the model will be integrated during the growing season until the time of the KEOPS measurements, at the end of the bloom.

The growing season has been estimated to last 85 day, based on satellite images and modelling (Mongin et al., 2008), and to end at the time of the KEOPS cruise. The sensitivity of the model to these choices will be discussed in Section 5.3.

4. Parameter estimation or how to quantify the processes

4.1. General strategy

An important objective of the current study is to use the model to make statements about the dominant processes responsible for the observed Si-isotopic distribution and to assign flux values to these processes. In this model each process is described by a single rate parameter. The question thus comes down to identifying and quantifying the non-zero rate parameters. If one wants to infer parameter values from a model-observation comparison, two general strategies can be followed. The first strategy is to "turn the (parameter) buttons" manually until a reasonable agreement is achieved between model and data. The alternative is to apply an inverse method to "objectively" match model and data to find the optimal parameter values. However, in the current case both strategies are problematic. Manual tuning is complicated because there are many parameters (18). Furthermore, guarantees about the robustness of the results are difficult because one cannot try all possible combinations. Unfortunately, we cannot apply an inverse method either, because the problem is ill-posed. Indeed, there are only very little data that can be used to infer the relatively high number of parameters. Therefore, we decided to use an intermediate approach, inspired by Brun et al. (2001). Note that in the following we will often simply refer to the rate parameters as "parameters".

Step 1: Propose parameter values for "total model" by manual tuning. By a first crude manual tuning, we assign first guess values to all 18 rate parameters. This "total model" will be the starting point for the next steps.

Step 2: Use prior knowledge to reduce the number of parameters to be estimated. For an inverse method to have any sense it is essential to reduce the number of parameters to be estimated. This means we have to neglect processes (i.e., set their parameter to zero) or to set some parameters in the total model to fixed values. This can be done by using prior knowledge under the form of independent estimates from previous studies or reasonable assumptions based on previous experience. If necessary, total model sensitivities can also be a valuable tool to decide which parameters can be kept constant, because they anyway do not influence the model results much. This step may seem logical (it is standard practice when tuning a model manually), but it has one important consequence: the prior knowledge is "used up" and cannot be used anymore to validate the model.

Table 4
Overview of rate parameter values used in the simulation, as well as the resulting integrated flux values and comparison to available literature values.

Process	Rate parameter				Flux integrated over 85 days [moles/m^2]			
	Symbol [units]	Value total model (all tuned)	Value model 1 (*=fixed)	Value model 2 (*=fixed)	Total model	Model 1	Model 2	External estimate
Uptake box 1	k_{U1} [d^{-1}]	2.4e−12	2.4e−12*	3.1e−12	6.0	4.8	5.0	0.2–4.7[a]
Uptake box 2	k_{U2} [d^{-1}]	4.8e−14	0*	0*	1.8	/	/	n.a.
Uptake box 3	k_{U3} [d^{-1}]	2.8e−13	2.8e−13*	2.8e−13	5.2	5.8	5.8	0.2–4.7[a]
Uptake box 4	k_{U4} [d^{-1}]	1.4e−14	0*	0*	1.3	/	/	n.a.
Dissolution box 1	k_{D1} [d^{-1}]	0.022	0.022*	0.022*	1.5	1.7	1.8	0.0–2.2[b]
Dissolution box 2	k_{D2} [d^{-1}]	0.009	0.009*	0.017	0.85	0.58	1.2	±0.5[c]
Dissolution box 3	k_{D3} [d^{-1}]	0.06	0.06*	0.06*	1.4	1.6	1.6	0.0–2.2[b]
Dissolution box 4	k_{D4} [d^{-1}]	0.01	0.01*	0.02	0.28	0.25	0.48	±0.5[c]
Sedimentation 1–2	k_{S12} [d^{-1}]	0.06	0.037	0.035	4.2	2.8	2.9	1.0–10.0[d]
Sedimentation 2↓	k_{S2x} [d^{-1}]	0.04	0.020	0.011	3.8	1.3	0.8	n.a.
Sedimentation 3–4	k_{S34} [d^{-1}]	0.16	0.15	0.15	3.6	4.0	4.0	1.0–10.0[d]
Sedimentation 4↓	k_{S4x} [d^{-1}]	0.15	0.14	0.14	4.2	3.5	3.3	n.a.
Mixing/advection 2-1	F_{21} [mol d^{-1}]	4e8	±0	0*	0.85	/	/	n.a.
Mixing/advection ↑2	F_{x2} [mol d^{-1}]	4e5	±0	0*	0.00085	/	/	n.a.
Mixing/advection 3–1	F_{31} [mol d^{-1}]	4e8	±0	0*	0.85 (in) 0.17 (out)	/	/	n.a.
Mixing/advection 4–2	F_{42} [mol d^{-1}]	4e8	±0	0*	0.85 (in) 0.17 (out)	/	/	n.a.
Mixing/advection 4–3	F_{43} [mol d^{-1}]	2.5e9	2.5e9*	2.5e9*	1.1	1.1	1.1	1.5–1.6[e]
Mixing/advection ↑4	F_{x4} [mol d^{-1}]	2.5e8	0*	0*	0.11	/	/	n.a.

[a] Treguer and van Bennekom (1991), Leynaert et al. (1993), Nelson et al. (1995), Pondaven et al. (2000), Nelson et al. (2002), Sigmon et al. (2002).
[b] Nelson and Gordon (1982), Brzezinski et al. (2001), Beucher et al. (2004).
[c] Nelson et al. (2002).
[d] Pondaven et al. (2000), Nelson et al. (2002), Jin et al. (2006), Pollard et al. (2006).
[e] Fripiat et al. (2011a), Fripiat et al. (2011b).

Step 3: Optimise reduced set of model parameters. If the model reduction in step 2 was done well, the remaining set of unknown parameters should be identifiable (well-posed problem). In that case it is possible to find one (or a finite number) of optimal values for these parameters. These can be found by many different optimisation methods. In this study we applied a Bayesian approach: the marginal probability distributions of the estimated parameters are reconstructed by performing a large number of Markov Chain Monte Carlo (MCMC) simulations in which the parameter values are randomly sampled (by perturbing the previous parameter set, and thus forming a "chain", Chib and Greenberg (1995)). The probability of every tested parameter set is evaluated by comparing the model output with the available measurements (at the end of the season) and their uncertainty (cf. Section 3.5). This analysis will provide a rational basis to assign values to the free model parameters.

Step 4: If necessary: repeat steps 2–3. If step 3 clearly shows that some parameters should actually be zero, it may be interesting to remove these parameters from the model and optimise another reduced parameter set.

More details on the application of each step are given in Section 5. It is crucial to keep in mind that we apply this procedure to enable an objective deconvolution of the considered processes (uptake, dissolution, settling, vertical mixing and horizontal exchange), a result which cannot be obtained by mere inspection of the Si-related data. By this quantitative model-data approach, it will be possible to identify the dominant processes acting on the KEOPS Si-isotopic data, i.e., which processes are not strictly necessary to reproduce the Si measurements.

4.2. Sensitivity measures

To help decide which parameters to estimate and which ones to keep to a constant value, the model sensitivity to varying parameter values is a useful tool (cf. step 2 above). In addition, parameter sensitivity analysis can help gain insights in the internal functioning of the model.

Two sensitivity measures were computed. In the first, we varied each model parameter around its calibration ("default") value (cf. Table 4), between a value $p_j^{\min}$ and a value $p_j^{\max}$ such that $p_j^{\max}-p_j^{\min}=rcp_j^{\text{default}}$. The isotopic fractionation factors for uptake and dissolution have also been varied. Then the effect of this parameter variation on each model output y_i can be measured by computing the following relative sensitivity measure:

$$S_{ij}^R=\frac{abs\left(y_i\left(p_j^{\max}\right)-y_i\left(p_j^{\min}\right)\right)}{y_i\left(p_j^{\text{default}}\right)} \tag{22}$$

The advantage of this measure is that it is rather intuitive. It allows to compare relative changes in parameters (r) with relative changes in output (S_{ij}^R). It will be referred to as "relative sensitivity" and the results are discussed in Section 4.2.1.

In the second sensitivity test we followed the approach suggested in Brun et al. (2001). In order to obtain dimensionless sensitivity information, they propose the following scaled sensitivity matrix

$$S_{ij}^S=\frac{\partial y_i(p^{\text{default}})}{\partial p_j}\frac{\Delta p_j}{SC_i}=J_{ij}\frac{\Delta p_j}{SC_i}, \tag{23}$$

where $y_i(p^{\text{default}})$ is the ith model output, obtained with parameter set p^{default}, p_j stands for the jth parameter which can be reasonably assumed to vary within a range Δp_j, and SC_i is a scale factor with the same physical dimension as y_i and should be chosen to have a typical value of y_i. $\frac{\partial y_i}{\partial p_j}$ is also referred to as the Jacobian matrix J_{ij}. As we do not have much prior knowledge on the parameters, we chose $\Delta p_j=p_j$ and for SC_i we took the mean value of the corresponding variable, i.e., $SC_i=\frac{y_i(t=0)+y_i(t=T)}{2}$. Note that the relative sensitivity measure presented in Eq. (21) is also dimensionless, and due to its "relative" nature, also takes into account in some way the different scales of the parameters and

output variables. If we sum the scaled sensitivities over all N outputs, we can compute a scaled sensitivity index for each parameter, e.g.,

$$S_j^{msqr} = \sqrt{\frac{1}{N}\sum_{i=1}^{N} S_{ij}^2}, \quad (24)$$

allowing a ranking of the parameters. By analogy with this procedure, we also summed the elements of the relative sensitivity matrix columns to get a "relative sensitivity index". We ranked the parameters of the "total model" according to both indices in order to help reduce the number of free parameters.

5. Results and discussion

5.1. Step-wise parameter identification

Before interpreting the final results, we will present in detail how we assigned values to the different rate parameters and how some processes were neglected based on the step-wise procedure proposed in Section 4.1.

5.1.1. Total model (step 1)

A first rough manual tuning of the whole rate parameter set provided reasonable agreement with the Si measurements (root mean square relative error or RMSRE=0.024). The chosen parameter values and resulting integrated fluxes are given in Table 4. The model produces a plausible time-evolution of the Si concentrations, isotopic composition and fluxes (results not shown). So we could have decided to stop the "tuning" here and it would have been quite satisfactory. However, we wanted to add some objectivity to the choice of parameter values and, even more, we wanted to investigate which processes were actually significant, i.e., "necessary" to find reasonable results (in terms of Si).

5.1.2. First model reduction: Model 1 (step 2)

After having found a reasonable total parameter set, we used external knowledge to fix as many parameters as necessary to keep a parameter set that is identifiable. The Jacobian matrix of the total model has a rank of 8, indicating that at most 8 out of the 18 parameters can be estimated independently. Therefore, we tried to assign fixed values to 10 parameters:

The first assumption that we made is that there is no subsurface uptake, i.e., $k_{U2}=k_{U4}=0$. Subsurface uptake was suggested by Fripiat et al. (2011b), but only when assuming "out-plateau WW" as initial conditions, which were not the conditions assumed here (cf. Section 3.6). Si-uptake has been reported below the euphotic layer by Brzezinski and Nelson (1989) but this seems unlikely to be a significant process at the seasonal scale.

- The surface uptake fluxes derived from the total model were in reasonable agreement with previous studies (cf. Table 4). So we decided to keep these parameters fixed to the initially tuned values. Different methods have been used to estimate gross and net annual production, including tracer experiments (^{30}Si and ^{32}Si), seasonal Si(OH)$_4$ depletion, independent natural Si-isotopic estimates and modelling studies (Treguer and van Bennekom, 1991; Leynaert et al., 1993; Nelson et al., 1995; Pondaven et al., 2000; Nelson et al., 2002; Sigmon et al., 2002; Jin et al., 2006; Pollard et al., 2006; Fripiat et al., 2011b). These studies reported an annual gross bSiO$_2$ production for the AZ varying between 0.2 and 4.7 mol Si m^{-2} (Table 4) and an annual net bSiO$_2$ production of 1 to 10 mol Si m^{-2}. Considering that the range of net production is larger than for gross production, it is clear that these estimates are subject to large uncertainty and/or variability. Possibly, gross bSiO$_2$ production may be underestimated because they are extrapolated from snapshot tracer studies. Therefore, we accept our total model uptake fluxes, although they are slightly higher than the literature range. Moreover, given the fertilization effect in the Kerguelen area it seems plausible that uptake fluxes are higher than other estimates for the AZ (e.g., Jin et al., 2006; Sokolov and Rintoul, 2007).
- For the dissolution parameters, the same reasoning was followed; hence, their values were also kept fixed to the initially tuned values (Table 4).
- Again the same reasoning was followed for F_{43} (Table 4). The resulting vertical Si-supply in the "out plateau" area (1.1 mol Si m^{-2}) is undistinguishable from the independent Si-isotopic estimate from Fripiat et al. (2011b) (1.5 $\pm$ 0.7 mol Si m^{-2}).
- At least one more rate parameter had to be fixed. For this, we investigated the ranking of the 18 parameters according to the two sensitivity indices (for the total model) defined in Section 4.2; these rankings are shown in Fig. 6. Finally, F_{x4} was set to zero, because it is already quite small and the model appears to be hardly sensitive to this parameter.

After this (three processes removed and seven parameters set to fixed values), eight parameters remain to be estimated (see Fig. 3b for schematic). The according reduced Jacobian matrix is of full rank, meaning that the remaining parameters should be identifiable.

5.1.3. Model 1 parameter optimisation (step 3)

Fig. 7 shows the probability density distributions related to the free parameters in model 1. The parameter values giving the highest probability density have been reported in Table 4. However, Fig. 7 also illustrates that for each parameter a range of values provides reasonable results. For some parameters, this range is larger than for others, expressing the variable parameter uncertainty. The distribution (shape, mode, width) for each parameter depends on the model structure and on the uncertainty assigned to the measurements. This visualisation is interesting because it expresses the uncertainty associated with each parameter.

Surprisingly, four parameters exhibit a maximal probability for their value around zero: F_{12},F_{x2},F_{31} and F_{42}. This implies that the vertical mixing processes on the plateau and the lateral mixing/advection can be interpreted as non-significant. Note that we make no statement about whether or not these processes were occurring in reality, this analysis only allows to say that they did not significantly influence the Si observations at hand. Furthermore, as these parameters are also associated with a relative large range, non-zero values can also be used to produce realistic results. We must emphasize that these results are actual outcomes of the proposed model-data approach, and could not be obtained by mere inspection of the Si-related data alone. As in every modelling study, the results depend on the assumptions underlying the model structure (processes considered, parameterisations) and on the values "chosen" for the fixed model parameters, but the quasi-zero fluxes derived from Fig. 7 are not assumptions but model outcomes.

Having no vertical supply of Si(OH)$_4$ on the plateau may seem surprising, because it is assumed to be a major process for dissolved iron (Blain et al., 2008). The major difference is that surface waters are rich in Si(OH)$_4$ during (most of) the season, and hence vertical processes are hardly discernible. Furthermore, a negligible UCDW Si-supply (F_{x2}) during the growth period could

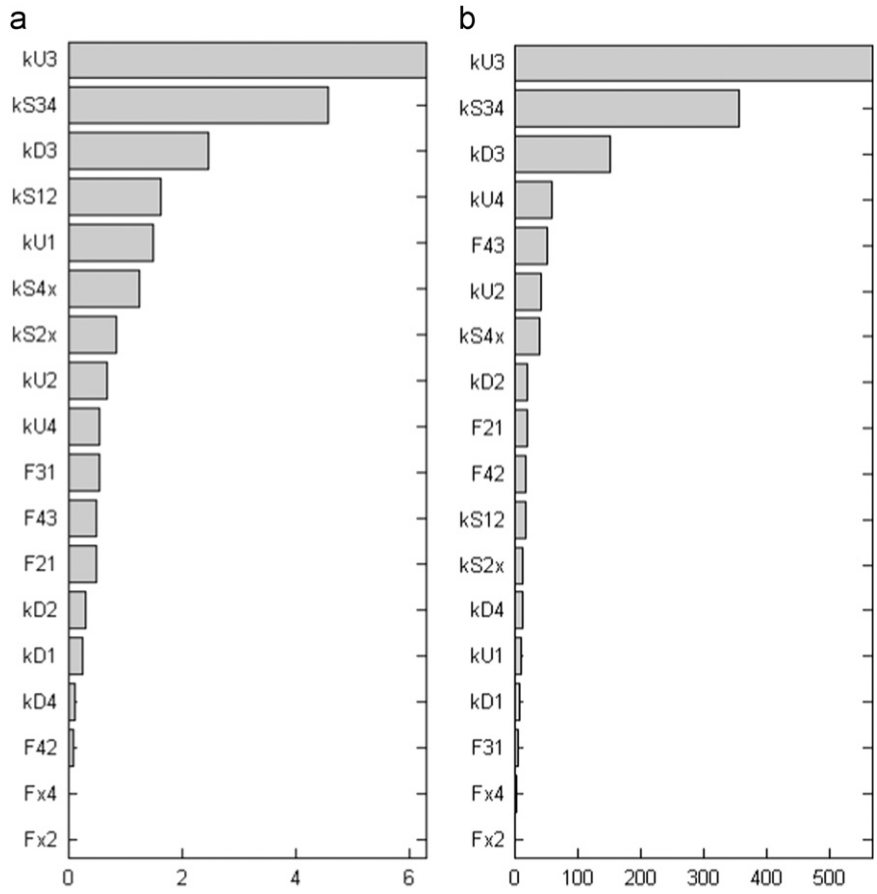

Fig. 6. Model parameters ranked according to their (a) relative and (b) scaled sensitivity index (for the total model).

be justified by the fact that the WW in the fertilized area (almost) reaches the seafloor (Park et al., 2008).

No lateral exchange between plateau and out-plateau boils down to having two separate vertical models, one for the "plateau" area and one for "out-plateau" (cf. Fig. 3c). This is partly contradictory to previous geochemical tracer studies on rare earth element (Zhang et al., 2008) and radium concentrations (van Beek et al., 2008), noticing a clear influence on the plateau of water with a signature similar to water close to Heard Island. Their hypothesis is that this water got its special signature by exchanging with sediments around Heard Island and was subsequently advected onto the plateau. Indeed, Si isotopes data also seemed to have recorded the impact of Heard Island plateau on δ^{30}Si signatures; however, such impact was limited to the surface signatures of one single station (C1, Fripiat et al., 2011b) and was not detected when looking at Si concentrations only. Our results suggest that for Si this mixing is not "necessary" to reproduce the plateau observations, probably because the dissolved concentrations are overwhelming in comparison to these external and local sources (e.g., Heard Island).

With the "most probable" parameter set, the RMSRE is 0.009. The simulated Si concentrations and isotopic compositions are shown and compared to the measurements in Fig. 8. The largest discrepancy between model and measurements is observed for $bSiO_2$-δ^{29}Si in box 3. The difference is $\sim$0.30‰, which is not excessive considering model oversimplifications and measurement uncertainties (cf. Sections 3.3 and 3.5). A different strategy to assign parameter values may improve the model fit in this box but will probably worsen the results elsewhere; therefore, it is not meaningful to discuss reasons for this slight misfit. This also implies that it is difficult to meaningfully improve the model, at least given the current dataset. Clearly, having additional measurement during the season would tremendously help to constrain the bloom peak and hence the rate parameters. This being said, the simulated bloom will be discussed in more detail in Section 5, together with the temporal evolution of the flux rates, shown in Fig. 9.

Note that the integrated fluxes associated with fixed first order parameters (denoted by "*k*") are different than in the total model setup. This follows from the fact that the fluxes are essentially integrated products of the rate parameter and concentrations; although the first may remain constant, the concentrations are affected by changes in other parameters and therefore the fluxes are also influenced.

5.1.4. *Second model reduction and parameter optimisation: model 2 (step 4)*

Given the (surprising) outcome that the most probable results are produced with 4 parameters set approximately to zero, we decided to perform a second estimation round. For model 2, we thus set four additional parameters to zero (cf. Fig. 3c) and this frees four more parameters that can now be estimated. Taking care that the new model 2 would again be identifiable (Jacobian matrix with rank 8), a new free parameter set was selected, now including two uptake and two dissolution rate parameters (cf. Fig. 3c or Table 4). The probability density samples for model 2 are shown in Fig. 10 and the parameters associated with the highest probability are listed in Table 4. This new analysis changes some of the parameter values, especially for k_{S2x} and

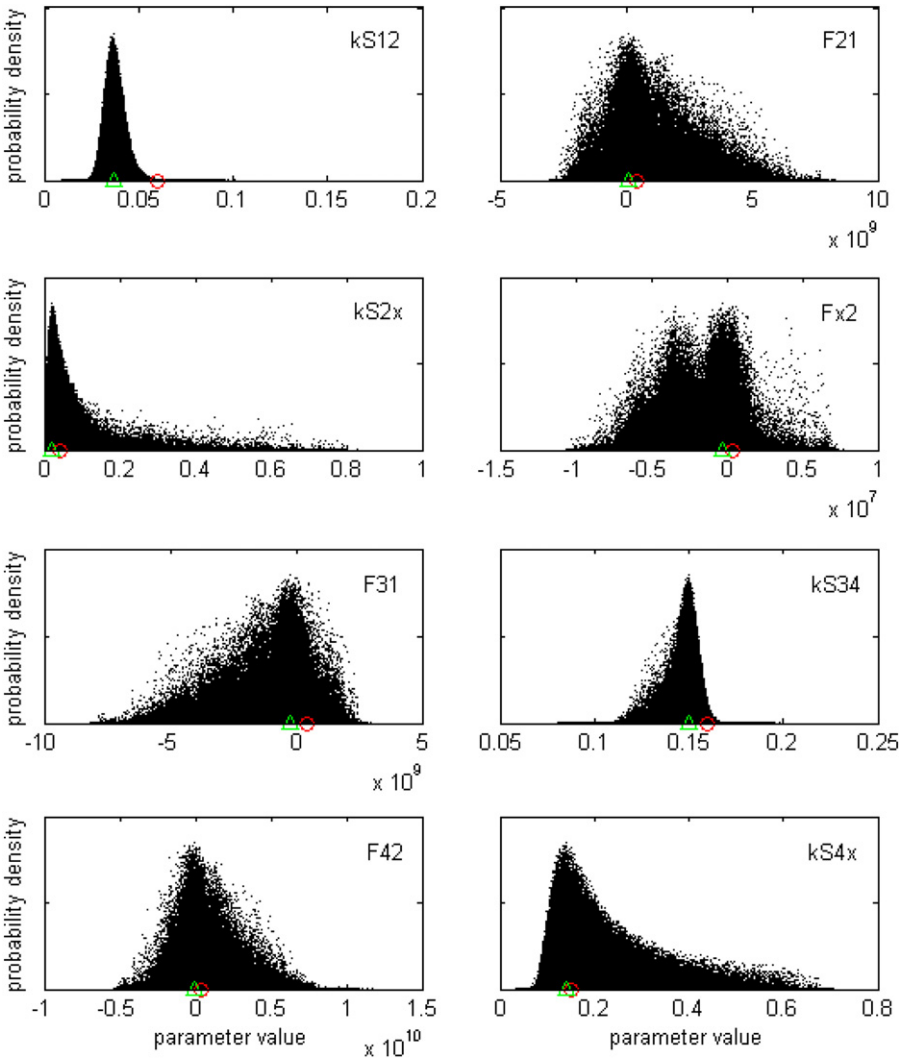

Fig. 7. Results of MCMC for the 8 free parameters in model 1. Each dot represents one simulation. Approximately 6e5 simulations were performed. The probability density axis has arbitrary units, so they are omitted. The red circle indicates the parameter value that was used in the total model, the green triangle is located at the parameter value associated with the highest probability. (For interpretation of the references to color in this figure legend, the reader is referred to the web version of this article.)

k_{U1}. The other settling and uptake parameters keep values similar to what was found for model 1. The "most probable" values for the dissolution parameters k_{D2} and k_{D4} (Table 4) are also different from what was used in model 1, but in Fig. 10 it can be seen that actually these parameters are not well defined. In other words, the values reported in Table 4 for k_{D2} and k_{D4} (model 2) are subject to large uncertainty and should not be interpreted quantitatively. This is probably related to numerical identifiability problems, and it is in line with the fact that for the total model these parameters were associated with relatively low sensitivity indices (Fig. 6).

The simulated time evolution with the optimised model 2 is hardly distinguishable from those obtained by model 1 (Fig. 8), and therefore is not shown. The RMSRE is 0.010, which is marginally larger than for model 1. This is just because the processes removed in model 2 did not have values exactly equal to zero in the optimised model 1 (Fig. 7). Although the model fit and the Si temporal evolution are hardly affected, the process fluxes are different, because the "most probable" values of some parameters changed between model 1 and 2 (Table 4). In other words, the instantaneous flux rates produced by the optimised model 2 are partly different from those presented for model 1 (Fig. 10). In fact, off the plateau both models produce quasi-identical results. On the plateau, the production peak is a few days earlier and more intense (maximum of about 0.3 mol m^{-2} d^{-1}) and therefore the surface silicic acid pool is depleted earlier and a "plateau" regime is reached from day 45, where the isotopic compositions and ratios of dissolution/production rates and export/production rates remain constant.

5.2. Discussion of the results

5.2.1. Bloom evolution

In this section, we want to discuss the simulated seasonal evolution of the bloom by inspection of the changing Si pools (Fig. 8) and fluxes (Fig. 9). Simulated Si-uptake matches relatively well with the expected $bSiO_2$ concentration evolution. On the plateau, [$bSiO_2$] (Fig. 8a) peaks around day 30, i.e., early December 2004, which is in agreement with previous reports based on satellite images of Chl-*a* (Mongin et al., 2008). Fig. 9a shows that the production peak on the plateau is approximately a week earlier. Outside the plateau, the peaks of $bSiO_2$ concentration and production occur later, around days 50–55, i.e., early January 2005. This is slightly later than suggested by remote sensing (although very variable, Mongin et al., 2008) but is quite similar to the timing simulated by a 1D

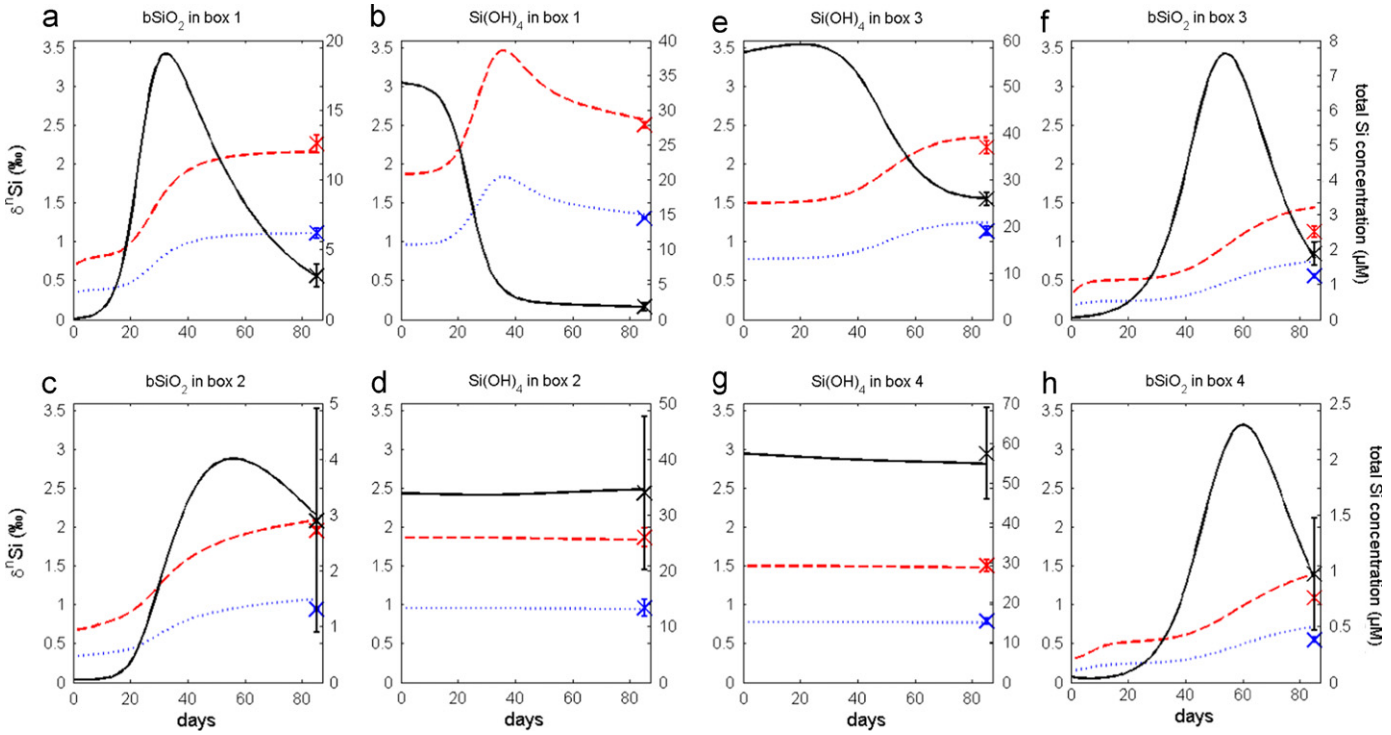

Fig. 8. Simulation evolution of δ^{29}Si (dotted blue) and δ^{30}Si (dashed red) and total [Si] (full black) for the "most probable" parameters of model 1 (Table 4) compared to the values measured at the end of the season (crosses for the medians and errorbars representing the interquartile ranges). Each plot represents one pool of the model and the plots are arranged as the pools in the schematic model in Fig. 3. (For interpretation of the references to color in this figure legend, the reader is referred to the web version of this article.)

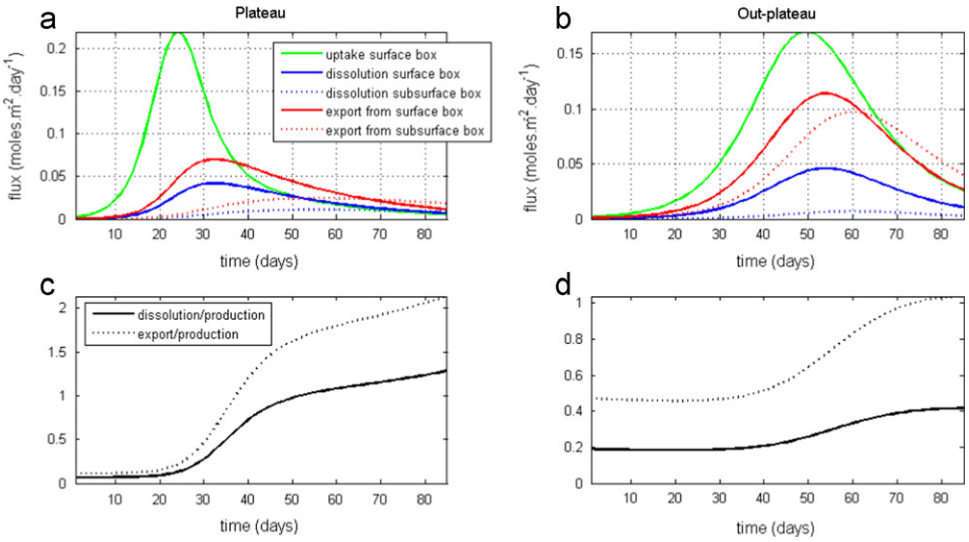

Fig. 9. Time evolution of the uptake (production), dissolution and export flux rates (a) and (c), as well as the associated ratios of dissolution/production and export/production (c) and (d). All results are obtained by model 1 with its "most probable" parameter set (cf. Table 1).

model for the KERFIX station (Pondaven et al., 1998). We decided not to use satellite Chl-*a* estimates as additional quantitatively constraining data in our model optimisation, because it would probably introduce more uncertainties than certainties. First of all, satellite Chl-*a* estimates themselves are highly uncertain, especially in the Southern Ocean (Dierssen, 2010). First, for our application it would require to transform the Chl-*a* into Si concentrations, implying assumptions on (time-varying) diatom proportion in the total phytoplankton pool, as well as Si content (and isotopic composition) of the diatoms. Second, the water depth for which the remote sensing Chl-*a* is representative is probably much shallower (5–10 m, cf. Smith, 1981) than our surface box (100 m). These considerations led us to restrict the use of remote sensing to more qualitative measures.

Note that when first-order kinetics were used (Eq. (8)) instead of second order (Eq. (9)) for the uptake terms, the off-plateau peak was simulated in a similar way (results not shown). However, it proved impossible to delay the plateau production peak for more than ~10 day after the simulation start, because the initial silicic acid concentrations are so high. By including a dependence on [$bSiO_2$] in the second-order formulation, the uptake rate is kept low as long as [$bSiO_2$] is weak, therefore delaying the production peak.

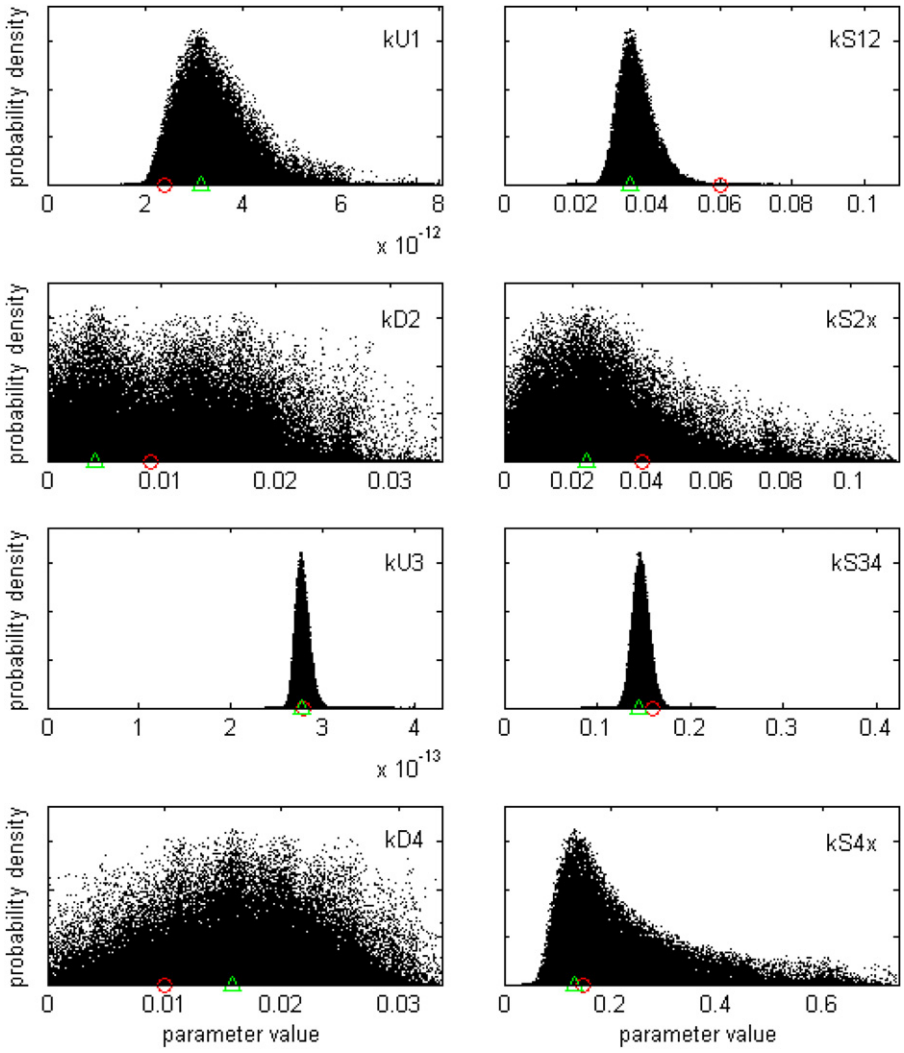

Fig. 10. Results of MCMC for the eight free parameters in model 2. Each dot represent one simulation. Approximately 1e5 simulations were performed for these results. The probability density axis has arbitrary units, so they are omitted. The red circle indicates the parameter value that was used in the total model, the green triangle is located at the parameter value associated with the highest probability. (For interpretation of the references to color in this figure legend, the reader is referred to the web version of this article.)

Both on and off the plateau, the [$bSiO_2$] increase follows a decrease in the dissolved Si pool, which is left enriched in heavy isotopes due to the isotopic fractionation during the uptake process (De La Rocha et al., 1997). As the dissolved pool becomes heavier, the $bSiO_2$ product also enriches in heavy isotope. On the plateau, the $Si(OH)_4$ is quickly depleted, causing the surface bloom to collapse. In addition, in both zones, dissolution and export to the subsurface layer (Fig. 9a and c) cause the surface [$bSiO_2$] to decrease. The export brings $bSiO_2$ to the subsurface layer, where the model simulates a peak shifted by ~6 (out-plateau)—25 (plateau) days and broadened, reflecting the delay effects of the settling process. The model suggests that the export off-plateau occurs at a higher rate (Table 4 and Fig. 9), explaining the much shorter delay in this zone. The subsurface peak of $bSiO_2$ also decreases as it is progressively exported further down. The subsurface dissolved Si pool is rather constant, both in terms of total concentration and isotopic signature, in agreement with observations (Pondaven et al., 2000; Altabet and Francois, 2001). This is due to (i) the initial conditions taken to be identical to the final KEOPS measurements, (ii) the absence of subsurface uptake in the model, and (iii) the small impact of mixing/advection/dissolution on these large subsurface pools on a seasonal timescale.

5.2.2. *Process fluxes*

The integrated flux values produced by the model are compared to literature values in Table 4. However, this comparison was already used to help assign first guess values to the parameters in model 1; therefore, it can really no longer be used as a real validation.

Uptake. The range of simulated instantaneous $bSiO_2$ production (Si-uptake) rates on the plateau (0 to 0.22 mol Si m^{-2} d^{-1}, Fig. 9a) and off the plateau (0 to 0.17 mol Si m^{-2} d^{-1}, Fig. 9b) are higher than previous studies south of the PF (0.00 to 0.09 mol Si m^{-2} d^{-1}; e.g., Ragueneau et al. (2000); updated with Brzezinski et al. (2001), Queguiner and Brzezinski (2002), Beucher et al. (2004), Mosseri et al. (2008)). The higher instantaneous Si-uptake rate on compared to off the plateau – or, more generally, than the iron-depleted Antarctic Zone – should be attributed to natural iron fertilization on and downstream of the Kerguelen Plateau (Blain et al., 2007; Mongin, 2008; Sokolov Rintoul, 2007). There is clear evidence that the rate of Si-uptake is regulated by the ambient iron concentration (e.g., Brzezinski et al., 2008; Mosseri et al., 2008), i.e., the uptake rate constant on the plateau (k_{U1}) should be larger than off the plateau (k_{U3}), as it is in our study (Table 4).

A seemingly puzzling result of this modelling exercise is that the seasonally-integrated uptake flux above the plateau

is (slightly) lower than off the plateau, (see Table 4), while at first sight it might be expected that above the plateau more integrated production would occur due to the fertilization effect. However, this result can be explained by the following facts:

(1) The starting $Si(OH)_4$ concentration at the onset of the stratification, i.e., the winter mixed layer initial silicic acid stock, is significantly low on compared to off the plateau, (respectively 33.9 and 57.4 $\mu mol\, l^{-1}$, Table 3). Diatoms removed 32 $\mu mol\, l^{-1}$ of silicic acid in both areas (difference between the assumed initial and final mixed layer $Si(OH)_4$ concentration). As a result, the Si-depletion is nearly complete (1.8 $\mu mol\, l^{-1}$) on the plateau and achieved well before the end of the growth season, while it is only partial (25.9 $\mu mol\, l^{-1}$) off the plateau. Such depletion inhibits further production and considering that the seasonally-integrated Si-uptake increases with increasing $Si(OH)_4$ concentration (Eq. (20)), we can explain why the integrated production is lower on-plateau than off-plateau.
(2) Under Fe depletion Si:N uptake ratios of diatoms tend to be up to three times higher (Hutchins and Bruland, 1998; Takeda, 1998). This was confirmed by the observation that off-plateau diatoms are more silicified than on the plateau (Armand et al., 2008; Mosseri et al., 2008). Therefore, the relatively similar opal production suggested by our model analysis, is in agreement with a higher net community production on than off-plateau, as was previously reported based on a seasonal carbon budget (up to three times higher, Jouandet et al., 2008).

Dissolution and export. Very few studies measured the $bSiO_2$ dissolution in the surface waters of the Southern Ocean (Nelson and Gordon, 1982; Nelson et al., 1995; Brzezinski et al., 2001; Beucher et al., 2004; Fripiat et al., 2011c). The simulated $bSiO_2$ dissolution in the KEOPS area (Fig. 9, 0.00 to 0.05 mol Si $m^{-2}\, d^{-1}$) is compatible with previously reported estimates (0.00 to 0.06 mol Si $m^{-2}\, d^{-1}$; e.g., Ragueneau et al. (2000); updated with Brzezinski et al. (2001); Beucher et al. (2004)).

The Si-export from the mixed layer reflects the Si-uptake and subsequently was lower on than off plateau, respectively 2.9 and 4.0 mol m^{-2}. Taking the Jouandet et al. (2008) values for carbon export, we estimated a seasonal Si:C export ratio of 0.5 and 2.4 from the on and off plateau mixed layer. This is in the range of Si:C export south of the Polar Front given by Ragueneau et al. (2002). This lower Si:C exported on the plateau could be explained by (1) a less silicified diatom community (Armand et al., 2008; Mosseri et al., 2008), (2) a longer residence time for $bSiO_2$ in the mixed layer due to a lower export rate, and (3) a more efficient microbial foodweb on the plateau (Obernosterer et al., 2008). The latter should promote a more efficient biogenic silica dissolution by degrading the organic matrix which protects diatom frustules from dissolution (Bidle and Azam, 1999). Steps (2)) and (3) imply a more efficient silicate pump off than on plateau, i.e., a more efficient recycling of organic matter than biogenic silica (Dugdale et al., 1995).

To the best of our knowledge, Nelson et al. (2002) is the only study which reports an estimate of subsurface dissolution in the AZ: 64% of the $bSiO_2$ export at 100 m would reach 1000 m. Using this model for the Kerguelen area, we can also estimate which proportion of the $bSiO_2$ export at 100 m reached 400 m, (respectively 0.37, and 0.85 for on and off plateau). Similarly to the mixed layer, this suggests a less efficient silicate pump in the subsurface on the plateau (Dugdale et al., 1995). Together with the longer residence time of biogenic silica in the subsurface layer, such difference could result in a more efficient biogenic silica recycling in subsurface on plateau (as given by the model, Table 4), possibly reinforced by sediment resuspension too. This more efficient silica recycling on the plateau may be caused by its diatom community being composed of smaller, more delicate species, as compared to off the plateau (Armand et al., 2008).

It is hard to compare with previous estimates of sedimentation speeds in the area because here the settling only refers to the opal fraction of the particles present.

D:P ratio. Previous studies observed a clear seasonal pattern in the D:P ratios from 0.0 at the beginning of the growth period to >1.0 at the end (Nelson and Gordon, 1982; Brzezinski et al., 2001; Beucher et al., 2004; Fripiat et al., 2011c). This trend seems to be respected by the model even if the D:P ratio remains lower than 0.50 off the plateau (Fig. 9b and d). Nevertheless the seasonal average value vary from 0.25 to 0.36 and 0.26 to 0.28, for, respectively on and off the plateau, and these are all between the AZ estimate (0.20; Nelson et al. (2002)) and the global average (0.50; Brzezinski et al. (2003)).

Mixing/advection. It is difficult to validate our simulated mixing/advection fluxes (F_{ij}) with values from literature, because of their time-averaged, "net" nature. A puzzling result is that many of the mixing processes were not necessary to explain the observed Si distributions. The possible reasons for this result were already discussed in Section 5.1.3.

5.3. Sensitivity analysis

As already mentioned a few times, the presented model results are associated with high uncertainties. Therefore, we do not pretend that the outcomes should be interpreted quantitatively. Nevertheless, it is interesting to investigate the sensitivity of the presented results to the main choices made for the model setup.

Fig. 11 shows the results for the relative sensitivity measure (Eq. (21)), with parameters varied over the relatively wide range of $r=50\%$. Only for the fractionation factors, not their value but their difference from zero was varied over a range of 50%. For instance, α_U^{29} (default value in model was 0.9994) is varied from 0.99925 to 0.99955. The default simulation is the optimised model 1. Besides the rate parameters, the impacts of varying the values of the fractionation factors, the initial conditions, the simulation period (i.e., season period) and the volumes of the boxes is also considered.

Overall, it is clear that the model is not overly sensitive to changes in the rate parameter values, except for k_{U3}, clearly the most sensitive parameter. Varying k_{U3} by 50% causes a variation of 150% for $[Si(OH)_4]_{box\ 3}$. However, most variables react rather mildly on the parameter variations, which should give some confidence in the results being relatively robust, at least locally. The parameters causing insensitive outputs were generally set to zero.

The isotopic fractionation factors only influence the delta-values, as expected. However, they are not so sensitive, implying that the results obtained will still hold if the isotopic fractionation factors deviate slightly from the values assumed here. This is fortunate as the fractionation factors are still associated with quite some uncertainty (cf. Section 1). Changing the initial isotopic concentrations naturally influences the simulated final concentrations and isotopic compositions, but the overall effect is not overwhelming. The same holds for the assumed period of the growing season. Finally, varying the assumed box volumes has a linear effect, but only on the simulated total concentrations. Note that the model equations are independent of the box volumes, because the internal state variables are expressed in moles. The box volumes only come into play when transforming the isotopic moles into concentrations, which is only necessary for comparison with the measurements.

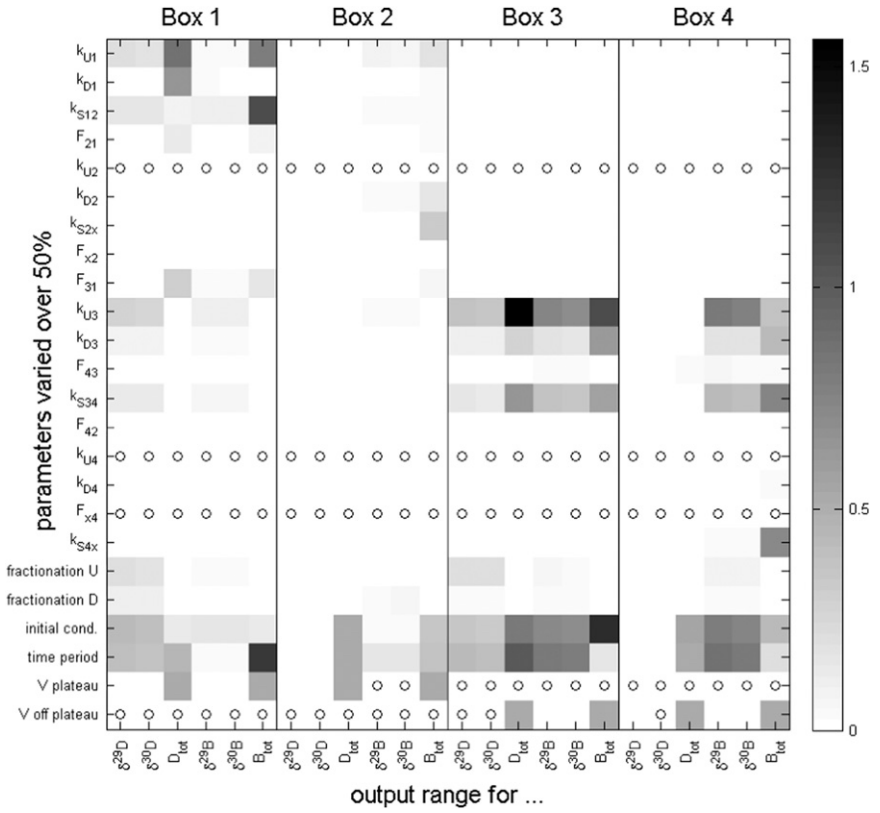

Fig. 11. Relative sensitivities of simulated concentrations and isotopic signatures in the different model boxes. Relative sensitivity is defined in Eq. 22. Parameters are varied over a 50% range ($r=0.5$) and colours express response range of the fluxes, concentrations and delta's. 'o' indicates that the relative sensitivity is exactly zero, distinguishing these values from "low" sensitivities (white colour).

When further inspecting Fig. 11, we can see which measurements would actually constrain the model parameter values. Remarkably, the parameters referring to processes in box 1 are mostly constrained by the total concentrations, rather than by the delta-values. However, this is not a general feature: the delta-values are seen to be informative for other parameters (e.g., k_{U3}, k_{D3}, k_{S34}). Yet, to improve the knowledge of the model parameters the main conclusion is that more measurements are needed.

If it were considered that measurements could be taken at one or several additional time moments, the current model could be a useful tool to determine which timing would produce most informative measurements (de Brauwere et al., 2009).

6. Conclusion and perspectives

We presented a box model describing the time evolution, both for concentration and isotopic composition, of dissolved and biogenic Si, simultaneously considering the processes of uptake, dissolution (both with isotopic fractionation), settling/export and mixing/advection. The setup presented is designed to describe the KEOPS situation where distinct "plateau" and "out-plateau" areas exist and were sampled. In addition, we distinguished between surface (0–100 m) and subsurface (100–400 m) water. This resulted in a model composed of 8 compartments, each containing three variables (the three natural Si isotopes) whose time evolution can be modelled. The model does not assume steady state, and uses information from natural recorders (concentration and isotopic composition) providing time-integrated signals about ecological processes in a tracer box model. This combination allows to go beyond instantaneous flux estimates and quantify integrated exchange fluxes during transient events like blooms. In the KEOPS case study the model simulated the 2004–2005 growth season, showing the growth peaks in each compartment and enabling both instantaneous and seasonally integrated estimates of the considered processes.

We intentionally kept the current model as simple as possible, with simple one-parameter process parameterizations and exclusion of dispensable processes. The (number of) available measurements did not justify increasing the complexity of the model. More measurements at one or more additional times during the season would indeed be extremely useful. They would allow reducing the uncertainty associated with the growth peaks and the initial conditions. More measurements in general would enable a more reliable determination of the rate parameter values, and a more quantitative identification of the significant processes (model selection) and of the best parameterization for each process (beyond single parameter parameterizations). We could also further refine the representation of the Si pools by making the distinction between living and detrital biogenic Si, with the first being involved in the production process and the latter in the dissolution process (each with its own isotopic fractionation).

The main reason for applying such a relatively simple model is that it potentially enables to estimate the importance of all included processes (uptake, dissolution, mixing and settling) at once. Ideally, an inverse approach could have provided the optimal rate parameter values by fitting the model to available (Si) observations. Unfortunately, the measurements are too scarce to allow an independent estimation of all rate parameters, and we therefore proposed an alternative, semi-objective procedure. Indeed, we believe that the limited observations should not be an excuse to restrain from modelling exercises, because they are –

notwithstanding the large uncertainties – irreplaceable tools to simultaneously assess the potential importance of different processes, and to compare different scenarios in a semi-quantitative way. Notwithstanding its relative simplicity, the model is able to reproduce the KEOPS measurements satisfactorily. Although not all processes could be quantified simultaneously, the model-data approach identified some processes as insignificant to explain the observed Si-isotopic observations.

Some of these results appear contradictory to previous suggestions based on other geochemical tracers. However, Si is special because of its relatively high concentrations in the Antarctic Zone and it is strongly influenced by biological processes. Furthermore, conclusions are always model-dependent and our model is different from the other analysis methods used. To really try and reconcile the different tracer observations, we believe a multi-tracer model should be built. The combination of tracers not only provides more data. Different tracers also constrain different processes, and an integrated multi-tracer model would allow to quantify all the processes simultaneously. The box model presented here could be a suitable tool for this kind of study. Its building blocks are generic and can be adapted for different tracers, different study domains or different time scales.

Acknowledgements

This work was conducted within the BELCANTO III network (contract SD/CA/03A of SPSDIII, Support Plan for Sustainable Development) funded by BELSPO, the Belgian Science Policy. The data used were obtained in the framework of the KEOPS project (ANR/INSU, PI: S. Blain, chief scientist: B. Quéguiner). Luc André thanks the FNRS for its financial support (FRFC project 2.4512.00). A. de Brauwere and F. Fripiat are post-doctoral researchers with the "Fonds National de la Recherche Scientifique" (FNRS, Belgium).

References

Abraham, K., Opfergelt, S., Fripiat, F., Cavagna, A.J., de Jong, J.T.M., Foley, S.F., Andre, L., Cardinal, D, 2008. Delta Si-30 and delta Si-29 determinations on USGS BHVO-1 and BHVO-2 reference materials with a new configuration on a nu plasma multi-collector ICP-MS. Geostand. Geoanal. Res. 32 (2), 193–202.

Alleman, L.Y., Cardinal, D., Cocquyt, C., Plisnier, P.D., Descy, J.P., Kimirei, I., Sinyinza, D., Andre, L., 2005. Silicon isotopic fractionation in Lake Tanganyika and its main tributaries. J. Great Lakes Res. 31 (4), 509–519.

Altabet, M.A., Francois, R., 2001. Nitrogen isotope biogeochemistry of the Antarctic Polar Frontal Zone at 170°W. Deep Sea Res. II 48 (19-20), 4247–4273.

Armand, L.K., Cornet-Barthaux, V., Mosseri, J., Queguiner, B., 2008. Late summer diatom biomass and community structure on and around the naturally iron-fertilised Kerguelen Plateau in the Southern Ocean. Deep Sea Res. Part II 55 (5-7), 653–676.

Beucher, C.P., Treguer, P., Corvaisier, R., Hapette, A.M., Elskens, M., 2004. Production and dissolution of biosilica, and changing microphytoplankton dominance in the Bay of Brest (France). Mar. Ecol. Prog. Ser. 267, 57–69.

Beucher, C.P., Brzezinski, M.A., Jones, J.L., 2008. Sources and biological fractionation of Silicon isotopes in the Eastern Equatorial Pacific. Geochim. Cosmochim. Acta 72 (13), 3063–3073.

Bidle, K.D., Azam, F., 1999. Accelerated dissolution of diatom silica by marine bacterial assemblages. Nature 397 (6719), 508–512.

Blain, S., Queguiner, B., Armand, L., Belviso, S., Bombled, B., Bopp, L., Bowie, A., Brunet, C., Brussaard, C., Carlotti, F., Christaki, U., Corbiere, A., Durand, I., Ebersbach, F., Fuda, J.L., Garcia, N., Gerringa, L., Griffiths, B., Guigue, C., Guillerm, C., Jacquet, S., Jeandel, C., Laan, P., Lefevre, D., Lo Monaco, C., Malits, A., Mosseri, J., Obernosterer, I., Park, Y.H., Picheral, M., Pondaven, P., Remenyi, T., Sandroni, V., Sarthou, G., Savoye, N., Scouarnec, L., Souhaut, M., Thuiller, D., Timmermans, K., Trull, T., Uitz, J., van Beek, P., Veldhuis, M., Vincent, D., Viollier, E., Vong, L., Wagener, T., 2007. Effect of natural iron fertilization on carbon sequestration in the Southern Ocean. Nature 446 (7139), U1070–U1071.

Blain, S., Sarthou, G., Laan, P., 2008. Distribution of dissolved iron during the natural iron-fertilization experiment KEOPS (Kerguelen Plateau, Southern Ocean). Deep Sea Res. II 55 (5-7), 594–605.

Brun, R., Reichert, P., Kunsch, H.R., 2001. Practical identifiability analysis of large environmental simulation models. Water Resour. Res. 37 (4), 1015–1030.

Brzezinski, M.A., Nelson, D.M., 1989. Seasonal-changes in the silicon cycle within a gulf-stream warm-core ring. Deep Sea Res. Part I 36 (7), 1009–1030, Papers.

Brzezinski, M.A., Nelson, D.M., Franck, V.M., Sigmon, D.E., 2001. Silicon dynamics within an intense open-ocean diatom bloom in the Pacific sector of the Southern Ocean. Deep Sea Res. II 48 (19-20), 3997–4018.

Brzezinski, M.A., Jones, J.L., Bidle, K.D., Azam, F., 2003. The balance between silica production and silica dissolution in the sea: insights from Monterey Bay, California, applied to the global data set. Limnol. Oceanogr. 48 (5), 1846–1854.

Brzezinski, M.A., Dumousseaud, C., Krause, J.W., Measures, C.I., Nelson, D.M., 2008. Iron and silicic acid concentrations together regulate Si uptake in the equatorial Pacific Ocean. Limnol. Oceanogr. 53 (3), 875–889.

Buesseler, K.O., Ball, L., Andrews, J., Cochran, J.K., Hirschberg, D.J., Bacon, M.P., Fleer, A., Brzezinski, M., 2001. Upper ocean export of particulate organic carbon and biogenic silica in the Southern Ocean along 170 degrees W. Deep Sea Res. II 48 (19-20), 4275–4297.

Cardinal, D., Alleman, L.Y., de Jong, J., Ziegler, K., Andre, L., 2003. Isotopic composition of silicon measured by multicollector plasma source mass spectrometry in dry plasma mode. J. Anal. At. Spectrom. 18 (3), 213–218.

Cardinal, D., Savoye, N., Trull, T.W., Dehairs, F., Kopczynska, E.E., Fripiat, F., Tison, J.L., Andre, L., 2007. Silicon isotopes in spring Southern Ocean diatoms: large zonal changes despite homogeneity among size fractions. Mar. Chem. 106 (1-2), 46–62.

Cavagna, A.-J., Elskens, M., Griffiths, F.B., Fripiat, F., Jacquet, S.H.M., Westwood, K.J., Dehairs, F., 2011a. Contrasting regimes of production and potential for carbon export in the Sub-Antarctic and Polar Frontal Zones South of Tasmania. Deep Sea Res. Part II 58 (21-22), 2235–2247.

Cavagna, A.J., Fripiat, F., Dehairs, F., Wolf-Gladrow, D., Cisewski, B., Savoye, N., Andre, L., Cardinal, D, 2011b. Silicon uptake and supply during a Southern Ocean iron fertilization experiment (EIFEX) tracked by Si isotopes. Limnol. Oceanogr. 56 (1), 147–160.

Chib, S., Greenberg, E., 1995. Understanding the Metropolis–Hastings algorithm. The American Statistician 49 (4), 327–335.

Daszykowski, M., Kaczmarek, K., Vander Heyden, Y., Walczak, B., 2007. Robust statistics in data analysis—a review: Basic concepts. Chemometr. Intell. Lab. 85 (2), 203–219.

de Brauwere, A., De Ridder, F., Elskens, M., Schoukens, J., Pintelon, R., Baeyens, W., 2005. Refined parameter and uncertainty estimation when both variables are subject to error. Case study: estimation of Si consumption and regeneration rates in a marine environment. J. Mar. Syst. 55 (3-4), 205–221.

de Brauwere, A., De Ridder, F., Gourgue, O., Lambrechts, J., Comblen, R., Pintelon, R., Passerat, J., Servais, P., Elskens, M., Baeyens, W., Kärnä, T., de Brye, B., Deleersnijder, E., 2009. Design of a sampling strategy to optimally calibrate a reactive transport model: exploring the potential for *Escherichia coli* in the Scheldt Estuary. Environ. Modell. Softw. 24 (8), 969–981.

De La Rocha, C.L., Brzezinski, M.A., DeNiro, M.J., 1997. Fractionation of silicon isotopes by marine diatoms during biogenic silica formation. Geochim. Cosmochim. Acta 61 (23), 5051–5056.

Demarest, M.S., Brzezinski, M.A., Beucher, C.P., 2009. Fractionation of silicon isotopes during biogenic silica dissolution. Geochim. Cosmochim. Acta 73 (19), 5572–5583.

Dierssen, H.M., 2010. Perspectives on empirical approaches for ocean color remote sensing of chlorophyll in a changing climate. Proc. Nat. Acad. Sci. U.S.A. 107 (40), 17073–17078.

Dugdale, R.C., Goering, J.J., 1967. Uptake of new and regenerated forms of nitrogen in primary productivity. Limnol. Oceanogr. 12 (2), 196–206.

Dugdale, R.C., Wilkerson, F.P., Minas, H.J., 1995. The role of a silicate pump in driving new production. Deep Sea Res. Part I 42 (5), 697–719, Papers.

Elskens, M., Baeyens, W., Cattaldo, T., Dehairs, F., Griffiths, B., 2002. N uptake conditions during summer in the SubAntarctic and polar frontal zones of the Australian sector of the Southern Ocean. J. Geophys. Res. Oceans 107 (C11), http://dx.doi.org/10.1029/2001JC000897.

Elskens, M., Baeyens, W., Brion, N., De Galan, S., Goeyens, L., de Brauwere, A., 2005. Reliability of *N* flux rates estimated from N-15 enrichment and dilution experiments in aquatic systems. Global Biogeochem. Cycles 19 (4), GB4028, http://dx.doi.org/10.1029/2004GB002332.

Elskens, M., de Brauwere, A., Beucher, C., Corvaisier, R., Savoye, N., Treguer, P., Baeyens, W., 2007. Statistical process control in assessing production and dissolution rates of biogenic silica in marine environments. Mar. Chem. 106 (1-2), 272–286.

Fripiat, F., Cavagna, A.J., Dehairs, F., Speich, S., André, L., Cardinal, D, 2011a. Silicic acid pools dynamics in the Antarctic Circumpolar current inferred from Si-isotopes. Ocean Sci. 8, 533–547.

Fripiat, F., Cavagna, A.J., Savoye, N., Dehairs, F., Andre, L., Cardinal, D, 2011b. Isotopic constraints on the Si-biogeochemical cycle of the Antarctic zone in the Kerguelen area (KEOPS). Mar. Chem. 123 (1-4), 11–22.

Fripiat, F., Leblanc, K., Elskens, M., Cavagna, A.-J., Armand, L., André, L., Dehairs, F., Cardinal, D., 2011c. Efficient silicon recycling in summer in both the Polar Frontal and Subantarctic Zones of the Southern Ocean. Mar. Ecol. Prog. Ser. 435, 47–61.

Fripiat, F., Cavagna, A.J., Dehairs, F., de Brauwere, A., André, L., Cardinal, D, 2012. Processes controlling Si-isotopic composition in the Southern Ocean for an application in paleoceanography. Biogeosciences 9, 1–15, http://dx.doi.org/10.5194/bg-5199-5191-2012.

Georg, R.B., Halliday, A.N., Schauble, E.A., Reynolds, B.C., 2007. Silicon in the Earth's core. Nature 447 (7148), 1102–1106.

Honjo, S., Manganini, S.J., Krishfield, R.A., Francois, R., 2008. Particulate organic carbon fluxes to the ocean interior and factors controlling the biological pump: a synthesis of global sediment trap programs since 1983. Prog. Oceanogr. 76 (3), 217–285.

Hutchins, D.A., Bruland, K.W., 1998. Iron-limited diatom growth and Si: N uptake ratios in a coastal upwelling regime. Nature 393 (6685), 561–564.

Jin, X., Gruber, N., Dunne, J.P., Sarmiento, J.L., Armstrong, R.A., 2006. Diagnosing the contribution of phytoplankton functional groups to the production and export of particulate organic carbon, CaCO(3), and opal from global nutrient and alkalinity distributions. Global Biogeochem. Cycles 20 (2), GB2015, http://dx.doi.org/10.1029/2005GB002532.

Jouandet, M.P., Blain, S., Metzl, N., Brunet, C., Trull, T.W., Obernosterer, I., 2008. A seasonal carbon budget for a naturally iron-fertilized bloom over the Kerguelen Plateau in the Southern Ocean. Deep Sea Res. Part II 55 (5-7), 856–867.

Krause, J.W., Nelson, D.M., Lomas, M.W., 2010. Production, dissolution, accumulation, and potential export of biogenic silica in a Sargasso Sea mode-water eddy. Limnol. Oceanogr. 55 (2), 569–579.

Leynaert, A., Nelson, D.M., Queguiner, B., Treguer, P., 1993. The silica cycle in the Antarctic Ocean—is the Weddell Sea atypical? Mar. Ecol. Prog. Ser. 96 (1), 1–15.

Martin-Jezequel, V., Hildebrand, M., Brzezinski, M.A., 2000. Silicon metabolism in diatoms: implications for growth. J. Phycol. 36 (5), 821–840.

Matsumoto, K., Sarmiento, J.L., 2008. A corollary to the silicic acid leakage hypothesis. Paleoceanography 23, 2.

Milligan, A.J., Varela, D.E., Brzezinski, M.A., Morel, F., 2004. Dynamics of silicon metabolism and silicon isotopic discrimination in a marine diatom as a function of pCO(2). Limnol. Oceanogr. 49 (2), 322–329.

Mongin, M., Molina, E., Trull, T.W., 2008. Seasonality and scale of the Kerguelen Plateau phytoplankton bloom: a remote sensing and modeling analysis of the influence of natural iron fertilization in the Southern Ocean. Deep Sea Res. II 55 (5-7), 880–892.

Mosseri, J., Quéguiner, B., Armand, L., Cornet-Barthaux, V., 2008. Impact of iron on silicon utilization by diatoms in the Southern Ocean: a case study of Si/N cycle decoupling in a naturally iron enriched area. Deep Sea Res. II 55, 801–819.

Nelson, D.M., Goering, J.J., 1977a. A stable isotope tracer method to measure silicic acid uptake by marine phytoplankton. Anal. Biochem. 78 (1), 139–147.

Nelson, D.M., Goering, J.J., 1977b. Near-surface silica dissolution in the upwelling region off northwest Africa. Deep Sea Res. 24 (1), 65–73.

Nelson, D.M., Gordon, L.I., 1982. Production and pelagic dissolution of biogenic silica in the Southern Ocean. Geochim. Cosmochim. Acta 46 (4), 491–501.

Nelson, D.M., Treguer, P., Brzezinski, M.A., Leynaert, A., Queguiner, B., 1995. Production and dissolution of biogenic silica in the ocean—revised global estimates, comparison with regional data and relationship to biogenic sedimentation. Global Biogeochem. Cycles 9 (3), 359–372.

Nelson, D.M., Anderson, R.F., Barber, R.T., Brzezinski, M.A., Buesseler, K.O., Chase, Z., Collier, R.W., Dickson, M.L., Francois, R., Hiscock, M.R., Honjo, S., Marra, J., Martin, W.R., Sambrotto, R.N., Sayles, F.L., Sigmon, D.E., 2002. Vertical budgets for organic carbon and biogenic silica in the Pacific sector of the Southern Ocean, 1996–1998. Deep Sea Res. II 49 (9-10), 1645–1674.

Obernosterer, I., Christaki, U., Lefèvre, D., Catala, P., Van Wambeke, F., Lebaron, P., 2008. Rapid bacterial mineralization of organic carbon produced during a phytoplankton bloom induced by natural iron fertilization in the Southern Ocean. Deep Sea Res. Part II 55 (5-7), 777–789.

Park, Y.H., Charriaud, E., Fieux, M., 1998. Thermohaline structure of the Antarctic Surface Water Winter Water in the Indian sector of the Southern Ocean. J. Mar. Syst. 17 (1-4), 5–23.

Park, Y.H., Roquet, F., Durand, I., Fuda, J.L., 2008. Large-scale circulation over and around the Northern Kerguelen Plateau. Deep Sea Res. II 55 (5-7), 566–581.

Pollard, R., Treguer, P., Read, J., 2006. Quantifying nutrient supply to the Southern Ocean. J. Geophys. Res. Oceans 111 (C5), C05011, http://dx.doi.org/10.1029/02005JC003076.

Pondaven, P., Fravalo, C., Ruiz-Pino, D., Treguer, P., Queguiner, B., Jeandel, C., 1998. Modelling the silica pump in the Permanently open Ocean zone of the Southern Ocean. J. Mar. Syst. 17 (1-4), 587–619.

Pondaven, P., Ragueneau, O., Treguer, P., Hauvespre, A., Dezileau, L., Reyss, J.L., 2000. Resolving the 'opal paradox' in the Southern Ocean. Nature 405 (6783), 168–172.

Queguiner, B., Brzezinski, M.A., 2002. Biogenic silica production rates and particulate organic matter distribution in the Atlantic sector of the Southern Ocean during austral spring 1992. Deep Sea Res. II 49 (9-10), 1765–1786.

Ragueneau, O., Treguer, P., Leynaert, A., Anderson, R.F., Brzezinski, M.A., DeMaster, D.J., Dugdale, R.C., Dymond, J., Fischer, G., Francois, R., Heinze, C., Maier-Reimer, E., Martin-Jezequel, V., Nelson, D.M., Queguiner, B., 2000. A review of the Si cycle in the modem ocean: recent progress and missing gaps in the application of biogenic opal as a paleoproductivity proxy. Global Planet. Change 26 (4), 317–365.

Ragueneau, O., Dittert, N., Pondaven, P., Tréguer, P., Corrin, L., 2002. Si/C decoupling in the world ocean: is the Southern Ocean different? Deep Sea Res. Part II 49 (16), 3127–3154.

Reynolds, B.C., Frank, M., Halliday, A.N., 2006. Silicon isotope fractionation during nutrient utilization in the North Pacific. Earth Planet. Sci. Lett. 244 (1-2), 431–443.

Reynolds, B.C., Aggarwal, J., Andre, L., Baxter, D., Beucher, C., Brzezinski, M.A., Engstrom, E., Georg, R.B., Land, M., Leng, M.J., Opfergelt, S., Rodushkin, I., Sloane, H.J., van den Boorn, S.H.J.M., Vroon, P.Z., Cardinal, D, 2007. An inter-laboratory comparison of Si isotope reference materials. J. Anal. At. Spectrom. 22 (5), 561–568.

Rosman, K.J.R., Taylor, P.D.P., 1998. Isotopic compositions of the elements 1997. J. Phys. Chem. Ref. Data 27 (6), 1275–1287.

Sarmiento, J.L., Gruber, N., Brzezinski, M.A., Dunne, J.P., 2004. High-latitude controls of thermocline nutrients and low latitude biological productivity. Nature 427 (6969), 56–60.

Sarmiento, J.L., Simeon, J., Gnanadesikan, A., Gruber, N., Key, R.M., Schlitzer, R., 2007. Deep ocean biogeochemistry of silicic acid and nitrate 21, 1Global Biogeochem. Cycles 21, 1.

Sigmon, D.E., Nelson, D.M., Brzezinski, M.A., 2002. The Si cycle in the Pacific sector of the Southern Ocean: seasonal diatom production in the surface layer and export to the deep sea. Deep Sea Res. II 49 (9-10), 1747–1763.

Smith, R.C., 1981. Remote sensing and depth distribution of ocean chlorophyll. Mar. Ecol. Prog. Ser. 5 (3), 359–361.

Sokolov, S., Rintoul, S.R., 2007. On the relationship between fronts of the Antarctic Circumpolar Current and surface chlorophyll concentrations in the Southern Ocean. J. Geophys. Res. Oceans 112 (C7), C07030, http://dx.doi.org/10.1029/02006JC004072.

Sokolov, S., Rintoul, S.R., 2009. Circumpolar structure and distribution of the Antarctic Circumpolar Current fronts: 1. Mean circumpolar paths. J. Geophys. Res. Oceans 114, C11018, http://dx.doi.org/10.1029/2008JC005108.

Takeda, S., 1998. Influence of iron availability on nutrient consumption ratio of diatoms in oceanic waters. Nature 393 (6687), 774–777.

Treguer, P., van Bennekom, A.J., 1991. The annual production of biogenic silica in the Antarctic Ocean. Mar. Chem. 35 (1-4), 477–487.

Treguer, P., Nelson, D.M., van Bennekom, A.J., Demaster, D.J., Leynaert, A., Queguiner, B., 1995. The silica in the world ocean—a reestimate. Science 268 (5209), 375–379.

Trull, T.W., Rintoul, S.R., Hadfield, M., Abraham, E.R., 2001. Circulation and seasonal evolution of polar waters south of Australia: Implications for iron fertilization of the Southern Ocean. Deep Sea Res. II 48, 2439–2466.

Uitz, J., Claustre, H., Griffiths, F.B., Ras, J., Garcia, N., Sandronie, V., 2009. A phytoplankton class-specific primary production model applied to the Kerguelen Islands region (Southern Ocean). Deep Sea Res. I 56 (4), 541–560.

van Beek, P., Bourquin, M., Reyss, J.L., Souhaut, M., Charette, M.A., Jeandel, C., 2008. Radium isotopes to investigate the water mass pathways on the Kerguelen Plateau (Southern Ocean). Deep Sea Res. II 55 (5-7), 622–637.

Varela, D.E., Pride, C.J., Brzezinski, M.A., 2004. Biological fractionation of silicon isotopes in Southern Ocean surface waters. Global Biogeochem. Cycles 18 (1), GB1047, http://dx.doi.org/10.1029/2003GB002140.

Watson, A.J., Garabato, A.C.N., 2006. The role of Southern Ocean mixing and upwelling in glacial–interglacial atmospheric CO_2 change. Tellus Ser. B: Chem. Phys. Meteorol. 58 (1), 73–87.

Young, E.D., Galy, A., Nagahara, H., 2002. Kinetic and equilibrium mass-dependent isotope fractionation laws in nature and their geochemical and cosmochemical significance. Geochim. Cosmochim. Acta 66 (6), 1095–1104.

Zhang, Y., Lacan, F., Jeandel, C., 2008. Dissolved rare earth elements tracing lithogenic inputs over the Kerguelen Plateau (Southern Ocean). Deep Sea Res. II 55 (5-7), 638–652.